Computer Methods in Applied Mechanics and Engineering 199 (2010) 2571–2589

Contents lists available at ScienceDirect

Computer Methods in Applied Mechanics and Engineering

journal homepage: www.elsevier.com/locate/cma

Mixed stabilized finite element methods in nonlinear solid mechanics Part II: Strain localization

M. Cervera *, M. Chiumenti, R. Codina

International Center for Numerical Methods in Engineering (CIMNE), Technical University of Catalonia (UPC), Edificio C1, Campus Norte, Jordi Girona 1-3, 08034 Barcelona, Spain

ARTICLE INFO

Article history:
Received 22 July 2009
Received in revised form 9 March 2010
Accepted 13 April 2010
Available online 21 April 2010

Keywords:
Mixed finite elements
Stabilization
Strain softening
Strain localization
Local damage models
Mesh dependence

ABSTRACT

This paper deals with the question of strain localization associated with materials which exhibit softening due to tensile straining. A standard local isotropic Rankine damage model with strain-softening is used as exemplary constitutive model. Both the irreducible and mixed forms of the problem are examined and stability and solvability conditions are discussed. Lack of uniqueness and convergence difficulties related to the strong material nonlinearities involved are also treated. From this analysis, the issue of local discretization error in the pre-localization regime is deemed as the main difficulty to be overcome in the discrete problem. Focus is placed on low order finite elements with continuous strain and displacement fields (triangular *P1P1* and quadrilateral *Q1Q1*), although the presented approach is very general. Numerical examples show that the resulting procedure is remarkably robust: it does not require the use of auxiliary tracking techniques and the results obtained do not suffer from spurious mesh-bias dependence.

1. Introduction

Strain localization occurs in softening materials subjected to monotonic straining. This phenomenon leads to the formation of *localization bands* inside the solid because, once the peak stress is reached within a band, and under further straining, strains concentrate inside the band while the material outside the band unloads elastically. Upon continuing straining, the localization progresses, the width of the localization band diminishes and, unless there is a physical limitation, it tends to zero. The particular components of the strain tensor that localize during this process depend on the specific constitutive behavior of the material. In Rankine-type materials, only normal elongations localize, eventually forming *tensile cracks*; in the so-called J_2 materials, shear (or slip) strains concentrate, leading to *slip surfaces (or lines)*.

It is generally accepted that the amount of energy released during the formation of a unit area of discontinuity surface is a material property, called the *fracture energy* (Mode I and Mode II fracture energies in Fracture Mechanics terminology). Dimensional analysis shows that if the elastic energy stored in the solid *volume* is released through the *area* of the fracture surface, the failure process leads to what is known as *structural size effect* [1]. Experimental evidence shows that, for a given structural geometry, ductile behavior is observed in the small scale limit, when the energy dissipated by inelastic behavior in the formation of the failure mechanism is much larger than the total stored elastic energy; contrariwise, brittle behavior occurs in the very large scale limit, when the ratio between the dissipated inelastic and available elastic energies is close to one. The small scale limit is suitable for small laboratory specimens, and the large scale limit is appropriate for structures of very large dimensions or even for scales larger than man-made structures. Thus, it is of practical interest to develop analytical and numerical tools suitable to bridge the gap between perfectly ductile and perfectly brittle behavior. This is called *quasi-brittle failure* [2].

Quasi-brittle failure has been the object of intensive interest in computational solid mechanics during the last four decades. Even if the main motivation for this interest is the wide range of engineering applications connected to this field, academic concern has been sharpened by the unexpected numerical difficulties encountered. The fact is that most attempts to model strain localization in softening materials with standard, irreducible, local approaches fail and that the solutions obtained suffer from mesh-bias dependence in such a strong manner that it cannot be ignored. Consequently, many different, alternative, strategies have been devised to model strain localization and quasi-brittle fracture and the references in the bibliography are uncountable. In the last 25 years, *micropolar* ([3,4]), *gradient-enhanced* ([5–9]) and *non-local*, ([5,10–14], among others) models have been proposed with the common basic idea of modifying the original continuous problem to introduce an internal length that acts as a localization limiter. On a different line, *viscous-regularized*, strain-

* Corresponding author.
E-mail address: miguel.cervera@upc.edu (M. Cervera).

0045-7825/$ – see front matter © 2010 Elsevier B.V. All rights reserved.
doi:10.1016/j.cma.2010.04.005

rate dependent models (see [5,13,15]) also attempt to solve the numerical difficulties by modifying the original continuous problem. Common to all these approaches there is the understanding that the underlying standard boundary value problem associated with quasi-brittle failure is not well posed and it must be reformulated. However, this standpoint ignores the well-known fact that "well-aligned" finite element meshes produce good results when using the standard (irreducible and local) approach. This evidence strongly suggests that the "flaw" that produces spurious mesh-bias dependence of the *discrete problem* is in the spatial discretization procedure.

In previous works, the authors have applied *stabilized mixed displacement–pressure methods* ([16–21] and [1]) to the solution of J_2 elasto-plastic and damage problems with simplicial elements. This formulation leads to a discrete problem which is fully stable, even for problems involving localization of shear strains and the formation of slip lines. The results obtained, both in terms of collapse mechanism and global load-deflection response, are practically *mesh independent*. In this paper, we make use of the *stabilized mixed strain–displacement method* presented in Part I [22] to extend these results to problems involving strain localization in Rankine-type materials and the formation of tensile cracks.

The outline of the paper is as follows. In the next section we briefly describe an isotropic Rankine damage model that is used throughout the paper as exemplary softening constitutive model to induce strain localization. Later, the problem of strain localization is discussed both in the irreducible and stabilized mixed forms, with emphasis on the obstacles posed by the nonlinear nature of the question. The difficulties on the nonlinear problem are illustrated in relation to a simple 1D problem. Next, the question of local discretization error in the pre- and post-peak regimes is analyzed for 2D problems, the role that the proposed mixed formulation plays in solving this error is described. Finally, two benchmark numerical examples involving finite elements meshes of linear triangles and bilinear quadrilaterals are discussed to assess the generality and robustness of the proposed formulation.

2. Isotropic Rankine damage model

The constitutive equation for the scalar isotropic damage model used in this work is:

$$\sigma = \mathbf{C} : \varepsilon = (1-d)\mathbf{C}_o : \varepsilon \tag{1}$$

where the stresses σ can be computed in terms of the total strain tensor ε, the linear elastic constitutive tensor $\mathbf{C}_o$, and the damage index d. Note that, being $\mathbf{C}_o$ positive definite, $\mathbf{C}$ is also positive definite for $d<1$.

The formulation of the damage model is completed with the definition of the evolution of the damage index in terms of the evolution of the total strains, or the effective stresses $\bar{\sigma}$, defined as $\bar{\sigma}=\mathbf{C}_o:\varepsilon$.

To model tensile damage, the equivalent effective stress, τ, is defined as:

$$\tau = \langle \bar{\sigma}_1 \rangle \tag{2}$$

where $\bar{\sigma}_1$ is the largest principal effective stress and $\langle\cdot\rangle$ are the Macaulay brackets ($\langle x\rangle = x$, if $x\geq 0$, $\langle x\rangle = 0$, if $x<0$).

The Rankine-type damage criterion, Φ, is then introduced as:

$$\Phi(\tau, r) = \tau - r \leq 0 \tag{3}$$

where r is an internal stress-like variable that is interpreted as the current damage threshold, in the sense that its value controls the size of the damage surface. The initial value of the damage threshold is $r_o = \sigma_o$, where σ_o is the initial uniaxial damage stress.

The (monotonic) expansion of the damage bounding surface for loading, unloading and reloading conditions is controlled by the Kuhn–Tucker relations and the damage consistency condition, which are

$$\dot{r} \geq 0 \quad \Phi(\tau, r) \leq 0 \quad \dot{r}\,\Phi(\tau, r) = 0 \tag{4a}$$

$$\text{if } \Phi(\tau, r) = 0 \text{ then } \dot{r}\,\dot{\Phi}(\tau, r) = 0 \tag{4b}$$

leading, in view of Eq. (3), to the loading condition

$$\dot{r} = \dot{\tau} \tag{5}$$

This leads to the explicit definition of the current values of the internal variable r in the form

$$r = max\{r_o, max(\tau)\} \tag{6}$$

The damage index is explicitly defined in terms of the corresponding current value of the damage threshold, $d = d(r)$, so that $\dot{d} = d'\dot{r} \geq 0$ and $0 \leq d < 1$. In this work, we will use the following exponential function:

$$d(r) = 1 - \frac{r_o}{r} exp\left\{-2H_S\left(\frac{r-r_o}{r_o}\right)\right\} \quad r_o \leq r \tag{7}$$

where $H_S \geq 0$ is the softening parameter.

The mechanical free energy is defined in the form:

$$W = (1-d)\,W^e(\varepsilon) = (1-d)\left[\frac{1}{2}\varepsilon : \mathbf{C}_o : \varepsilon\right] \geq 0 \tag{8}$$

Thus, the rate of mechanical dissipation can be expressed as

$$\mathcal{D} = W^e \dot{d} \geq 0. \tag{9}$$

In finite element implementations, in order to relate the specific dissipated energy $\mathcal{D}$, defined per unit volume, to the mode I fracture energy of the material $\mathcal{G}_f$, defined per unit area of damaged material, the *element characteristic length* l_{ch} ([23,24]) is introduced, so that

$$\mathcal{D} l_{ch} = \mathcal{G}_f. \tag{10}$$

For the damage model with exponential softening it can be proved that the specific dissipated energy is

$$\mathcal{D} = \left(1 + \frac{1}{H_S}\right)\frac{\sigma_o^2}{2E} \tag{11}$$

and, therefore, using Eqs. (11) and (12)

$$H_S = \frac{l_{ch}}{\overline{l}_S - l_{ch}} \geq 0 \tag{12}$$

where the *material length* is $\overline{l}_S = 1/\overline{H}_S$, with $\overline{H} = \sigma_o^2/(2E\mathcal{G}_f)$ depending only on the material properties. Note that this regularization procedure makes the softening modulus H_S, which defines the *discrete* local softening response, dependent on the elemental length l_{ch}.

For linear elements and in the irreducible formulation, the discrete localization band is only one element across, and the characteristic length is taken as the representative size of the element, $l_{ch} = h_e$. Note that the irreducible formulation corresponds to (see Part I [22]) $\tau_\varepsilon = 1$. For the non stabilized mixed problem ($\tau_\varepsilon = 0$), strain continuity implies a discrete localization band width of $l_{ch} = 2h_e$. In this work, we will assume $l_{ch} = (1-\tau_\varepsilon)2h_e + \tau_\varepsilon h_e$ for the stabilized mixed formulation, including the previous two limit cases. The size of the element will be computed as $h_e^2 = 2A_e$ for triangular elements and $h_e^2 = A_e$ for quadrilateral elements.

3. The problem of strain localization

In this section some relevant properties and difficulties associated to the strain localization problem are revised. To this end, we will consider first the irreducible formulation of the problem and later the stabilized mixed form of the same.

3.1. Irreducible form

3.1.1. Numerical stability and solvability

Let us consider first the strong and weak forms of the mechanical problem in the classical, irreducible, form.

The strong form of the problem can be stated as: find the displacement field $\mathbf{u}$, for given prescribed body forces $\mathbf{f}$, such that:

$$\nabla \cdot \sigma + \mathbf{f} = \mathbf{0} \quad \text{in } \Omega \tag{13}$$

where Ω is the open and bounded domain of $\mathbb{R}^{n_{\dim}}$ occupied by the solid in a space of n_{dim} dimensions. Eq. (13) is subjected to appropriate Dirichlet and Neumann boundary conditions. Without loss of generality, we will assume these in the form of prescribed displacements $\mathbf{u}=\mathbf{0}$ on $\partial\Omega_u$, and prescribed tractions $\bar{\mathbf{t}}$ on $\partial\Omega_t$, respectively.

Following the standard procedure, the corresponding *continuous* weak problem is

$$(\nabla^s \mathbf{v}, \sigma) = (\mathbf{v}, \mathbf{f}) + (\mathbf{v}, \bar{\mathbf{t}})_{\partial\Omega_t} \quad \forall \mathbf{v} \tag{14}$$

where $\mathbf{v} \in \mathcal{V}$ are the variations of the displacement field $\mathbf{u}$, $\mathcal{V}$ is a subspace of $H^1(\Omega)$, that is, the space of functions square integrable in Ω with square integrable derivatives and vanishing on $\partial\Omega_u$; $(\cdot,\cdot)$ denotes the inner product in $L^2(\Omega)$. Likewise, $(\mathbf{v}, \bar{\mathbf{t}})_{\partial\Omega_t}$ denotes the integral of $\mathbf{v}$ and $\bar{\mathbf{t}}$ over $\partial\Omega_t$.

This problem is rewritten in terms of the symmetric gradient of the displacements as

$$(\nabla^s \mathbf{v}, \mathbf{C} : \nabla^s \mathbf{u}) = (\mathbf{v}, \mathbf{f}) + (\mathbf{v}, \bar{\mathbf{t}})_{\partial\Omega_t} \quad \forall \mathbf{v} \tag{15}$$

By definition, Eq. (15) is *elliptic* if the secant tensor $\mathbf{C}$ is positive definite. For a scalar isotropic damage constitutive model, *ellipticity* is guaranteed for $d<1$.

A standard stability estimate for the linear version of problem (13) is obtained by multiplying the first term of the left hand side by $\mathbf{u}$ and integrating by parts over the domain Ω, to yield

$$(\nabla^s \mathbf{u}, \mathbf{C}_o : \nabla^s \mathbf{u}) = \|\mathbf{u}\|_E^2 \tag{16}$$

where $\|\cdot\|_E^2$ is the energy norm (equal to the elastic free energy). For strictly positive $\mathbf{C}_o$, the governing equation is *numerically stable*. Recall that a problem is stable when the solution can be shown to be bounded in terms of the data, applied forces and boundary conditions in this case.

For a scalar isotropic damage constitutive model, the stability estimate reads

$$(\nabla^s \mathbf{u}, (1-d)\mathbf{C}_o : \nabla^s \mathbf{u}) \geq c\, \|\mathbf{u}\|_E^2 \tag{17}$$

for a positive constant c, and numerical stability is guaranteed for $d<1$. Upon continuing straining, the damage index approaches 1 and the secant moduli may eventually vanish. However, inequality (17) *still holds* if the secant moduli vanish completely only in a subdomain $S \subset \Omega$ of zero measure. Note that the energy norm is defined in terms of total displacements, not their increments, and therefore, the use of the secant constitutive tensor is required.

The *discrete* version of the weak problem (15) is

$$(\nabla^s \mathbf{v}_h, \mathbf{C} : \nabla^s \mathbf{u}_h) = (\mathbf{v}_h, \mathbf{f}) + (\mathbf{v}_h, \bar{\mathbf{t}})_{\partial\Omega_t} \quad \forall \mathbf{v}_h \tag{18}$$

where $\mathbf{v}_h \in \mathcal{V}_h$ are the variations of the displacement field $\mathbf{u}_h$, $\mathcal{V}_h$ is a finite dimensional subspace of $\mathcal{V}$. The corresponding algebraic system of equations can be written as

$$\mathbf{K}(\mathbf{U})\mathbf{U} = \mathbf{F} \tag{19}$$

where the *secant* stiffness matrix $\mathbf{K}=\mathbf{K}(\mathbf{U})$ is defined from the bilinear form in Eq. (18).

In *linear* problems, numerical stability guarantees uniqueness of the solution. Moreover, for the irreducible formulation, the standard Galerkin discretization method provides a discrete problem which benefits from the elliptic nature of the continuous problem. This means that it is clear from Eq. (18) that $\mathbf{K}$ is *positive definite* if the constitutive matrix $\mathbf{C}$ is also positive definite. As a consequence, the system of Eq. (19) is *solvable* and its solution $\mathbf{U}$ is *unique*. This would be the situation when solving the damage mechanical problem for a given (frozen) distribution of damage, with $d<1$.

However, the strain localization damage problem is *nonlinear* because of the dependence of $\mathbf{C}$ (or d) on the displacements $\mathbf{u}$, and uniqueness of the solution cannot be proved as in the linear case. Despite that, some properties of the linear case are inherited by suitably defined linearized problems.

In practice, non linearity is dealt with assuming that the acting body forces and boundary tractions, $\mathbf{f}$ and $\bar{\mathbf{t}}$, are applied incrementally, being dependent on (pseudo)time or other loading parameters. Then, the problem is solved step-by-step in time (or load), and iterating within each step until equilibrium (Eq. (18)) is satisfied. For example, using Picard's method, a typical iteration (i) of such a (time) step for the corresponding problem would be

$$\left(\nabla^s \mathbf{v}_h, \mathbf{C}\left(\mathbf{u}_h^{(i-1)}\right) : \nabla^s \mathbf{u}_h^{(i)}\right) = (\mathbf{v}_h, \mathbf{f}) + (\mathbf{v}_h, \bar{\mathbf{t}})_{\partial\Omega_t} \quad \forall \mathbf{v}_h \tag{20}$$

This is a linearized equation for $\mathbf{u}_h^{(i)}$ and, therefore, if $d<1$, numerical stability guarantees that its solution $\mathbf{u}_h^{(i)}$ is *unique*. Similar conclusions could be drawn for other linearization strategies, such as a consistently derived Newton–Raphson scheme.

The corresponding linear algebraic system of equations would be

$$\mathbf{K}\left(\mathbf{U}^{(i-1)}\right)\mathbf{U}^{(i)} = \mathbf{F} \tag{21}$$

For $d<1$, the system of Eq. (21) is *solvable* and its solution $\mathbf{U}^{(i)}$ can be obtained. Therefore, once $\mathbf{U}^{(0)}$ and the iterative procedure (Picard's method in this case) are specified, and *if convergence is achieved*, a solution $\mathbf{U}$ is obtained. Nonetheless, different iterative procedures or different initial estimates may yield different solutions. This is discussed next.

3.1.2. Nonlinearity, convergence and uniqueness

Let us now consider in some detail the implications of the strain localization problem being *materially nonlinear*, because of the dependence of the constitutive tensor $\mathbf{C}$ (for instance, in the case of the isotropic damage model, through the dependence of the damage index d) on the (gradients of the) displacements $\mathbf{u}$.

The first implication is that uniqueness of solution is lost. For nonlinear problems, uniqueness of solution is an exceptional case; there are usually numerous solutions to the problem and they are usually path dependent, given that most material nonlinearities are non-reversible. Therefore, the previous arguments only prove that for a given (time) step, a given initial estimate and a given *convergent* iterative procedure, a certain solution is obtained.

This introduces a second implication: a convergent iterative procedure is required. In the previous discussion Picard's method was used because of its formal simplicity, but, in practice, other nonlinear algorithms are used. Considering the very popular Newton–Rahshon's method, or any of its modifications, the concept of consistent tangent stiffness matrix comes into play. Computing the tangent stiffness matrix involves the evaluation of the tangent constitutive tensor. But many nonlinear material processes are *sudden* and *irreversible* (like the onset and subsequent evolution of damage or plastic strains) and the corresponding constitutive models are written in terms of inequalities (such as the inelastic criteria and Kuhn–Tucker relations used in damage and plasticity models, see Eqs. (3) and (4a)) rather than equalities. This makes it necessary to distinguish between "loading" and "unloading" and this makes the mathematical concept of "tangent" not uniquely defined in most cases, even though strategies to overcome this problem have been proposed in specific situations ([25,26]). The same occurs when bounding surfaces present corners or apices. Also, the local material instability associated to strain softening makes tangent constitutive tensors non positive, introducing additional computational difficulties. All this amounts to the regrettable fact that achieving *satisfactorily converged* results in strongly material nonlinear problems is very difficult. If the intermediate solutions are not truly converged, the progressive *drift-off* error may lead to an unrealistic equilibrium path.

The third implication is the possible *loss of global structural stability*. To consider this, let us rewrite the constitutive tensor as

$$\mathbf{C} = \mathbf{C}_o + \mathbf{C}_m \tag{22}$$

where $\mathbf{C}_o$ is the linear elastic constitutive tensor, which is positive definite, and $\mathbf{C}_m = \mathbf{C}_m(\varepsilon)$ is the *material* nonlinear constitutive tensor. For the isotropic damage model used as exemplary case, $\mathbf{C}_m = -d(\varepsilon)\mathbf{C}_o$. Note that this tensor is negative definite. Using this split, Eq. (21) can be written as

$$\left[\mathbf{K}_o + \mathbf{K}_m\left(\mathbf{U}^{(i-1)}\right)\right]\mathbf{U}^{(i)} = \mathbf{F} \tag{23}$$

where $\mathbf{K}_o$ is the linear elastic stiffness matrix and $\mathbf{K}_m$ is the material nonlinear stiffness matrix. This format can be compared with the well known expression obtained for (elastic) *geometrically* nonlinear mechanical problems, which reads

$$\left[\mathbf{K}_o + \mathbf{K}_u\left(\mathbf{U}^{(i-1)}\right) + \mathbf{K}_g\left(\mathbf{U}^{(i-1)}\right)\right]\mathbf{U}^{(i)} = \mathbf{F} \tag{24}$$

where $\mathbf{K}_o$ is the linear elastic stiffness matrix, $\mathbf{K}_u$ is the nonlinear stiffness due to the consideration of finite displacements and $\mathbf{K}_g$ is the geometric nonlinear stiffness matrix. The comparison shows that the effect of increasing the values of the damage indices in the system (23), and the loss of local material instability implied in softening situations, is very similar to that of increasing the compressive (negative) stresses in the system (24): reducing the overall positivity (stability) of the system.

Applying standard linear stability techniques to the global equilibrium Eq. (23), with $\mathbf{F} = \lambda\bar{\mathbf{F}}$ and $\mathbf{K}_T(\mathbf{U}^{(i-1)})$ being the tangent stiffness matrix, results in the possibility of having critical (limit, bifurcation or turning) points in the equilibrium path if the equation

$$\mathbf{K}_T\left(\mathbf{U}^{(i-1)}\right)\Phi = \mathbf{0} \tag{25}$$

has non-trivial solutions. This implies that, depending on the sign of $|\mathbf{K}_T|$, global structural equilibrium at a point along the equilibrium path can be either strongly stable ($|\mathbf{K}_T|>0$), neutrally stable ($|\mathbf{K}_T|=0$) or unstable ($|\mathbf{K}_T|<0$). If $|\mathbf{K}_T|=0$ and $\dot{\lambda}=0$, the critical point is a limit point; if $|\mathbf{K}_T|=0$ and $\Phi^T\bar{\mathbf{F}}=0$, the critical point is a bifurcation point.

Other interesting points that may occur along the nonlinear equilibrium path are the turning points, where $|\mathbf{K}_T|=\infty$.

These situations occur regularly in problems involving strain localization, where loss of (local) material stability often leads to loss of (global) structural stability. Limit points are associated with peak loads and unstable branches are associated with post-peak states. Turning points may occur in situations where the ductility of the structure, that is, the relation between the energy necessary to develop the collapse mechanism and the stored elastic energy, is very small. This is why continuation methods such as displacement control or the arc-length, originally developed for geometrically nonlinear problems, are also very much used to solve potentially global unstable problems caused by strong material nonlinearities. Unfortunately, these methods are of little help in the case of bifurcation points, and this remains one of the main difficulties associated with strain localization problems, in the need of procedures for selecting the "appropriate" propagation track for the localization band.

A final implication regarding nonlinearity, lack of uniqueness and loss of global structural stability is the fact that the discrete system is only an approximation of the continuous one. In mathematical terms, the solution spaces for both problems are different. In more intuitive terms, the discrete system may be viewed as an "imperfect" version of the continuous one. This means that the solutions of both systems may differ significantly. In the best case, only some of the continuous solutions may be reflected on the discrete system (in a more or less approximate way) and some others will be lost in the discretization process (like bifurcation points are eliminated by imperfections). In the worst case, lack of numerical stability may cause that discrete solutions be spurious and unrelated to the continuous case. This last worst case is precisely what happens when a FE solution shows mesh-bias strain localization patterns.

3.2. Stabilized mixed form

3.2.1. Numerical stability and solvability

Let us now consider the *continuous mixed* ($\varepsilon/\mathbf{u}$) formulation of the problem. As stated in Part I of this work, in this case the associated weak form of the problem can be stated as:

$$-(\boldsymbol{\gamma}, \mathbf{C} : \varepsilon) + (\boldsymbol{\gamma}, \mathbf{C} : \nabla^s\mathbf{u}) = 0 \quad \forall\boldsymbol{\gamma} \tag{26a}$$

$$(\nabla^s\mathbf{v}, \mathbf{C} : \varepsilon) + (\mathbf{v}, \mathbf{f}) = 0 \quad \forall\mathbf{v} \tag{26b}$$

where $\mathbf{v} \in \mathcal{V}$ and $\boldsymbol{\gamma} \in \mathcal{G}$ are the variations of the displacements and strain fields, respectively. Let us assume, as before, that $\mathbf{C}$ is positive definite.

For this problem, numerical stability cannot be based only on ellipticity. However, for the *linear* problem stability and, therefore, existence and uniqueness of a solution $\mathbf{u} \in \mathcal{V}$, $\varepsilon \in \mathcal{G}$ can be proved if the spaces $\mathcal{V}$ and $\mathcal{G}$ satisfy a certain *inf-sup* condition.

The same arguments are valid for the *discrete mixed* ($\varepsilon_h/\mathbf{u}_h$) formulation of the problem if the Galerkin formulation is used: satisfaction of the *inf-sup* condition by the solution spaces $\mathcal{V}_h$ and $\mathcal{G}_h$ is necessary and sufficient to guarantee numerical stability and uniqueness of the solution. As satisfaction of the inf-sup condition is very stringent, an alternative consists of modifying the standard discrete form by adding the appropriate stabilization terms. This is the procedure followed in Part I of the paper. Once this is done, numerical stability can be assured and, therefore, *for a linear problem*, a solution $\mathbf{u}_h \in \mathcal{V}_h$, $\varepsilon_h \in \mathcal{G}_h$ exists and it is unique. This numerical stability issue is unrelated to material or structural instabilities that may arise in non-linear problems.

The corresponding stabilized algebraic system of equations can be written as (see Part I)

$$\begin{bmatrix} -\mathbf{M}_\tau & \mathbf{G}_\tau \\ \mathbf{G}_\tau^{\mathrm{T}} & \mathbf{K}_\tau \end{bmatrix} \begin{bmatrix} \mathbf{E} \\ \mathbf{U} \end{bmatrix} = \begin{bmatrix} 0 \\ \mathbf{F} \end{bmatrix} \tag{27}$$

or, formally rewritten as

$$\left[\mathbf{K}_\tau + \mathbf{G}_\tau^{\mathrm{T}} \mathbf{M}_\tau^{-1} \mathbf{G}_\tau\right] \mathbf{U} = \mathbf{F} \tag{28a}$$

$$\mathbf{E} = \left[\mathbf{M}_\tau^{-1} \mathbf{G}_\tau\right] \mathbf{U} \tag{28b}$$

where the global matrices $\mathbf{M}_\tau$, $\mathbf{G}_\tau$ and $\mathbf{K}_\tau$ come from the standard assembly procedure of the elemental contributions.

It follows from the stability analysis in Part I of this work that, if the constitutive matrix $\mathbf{C}$ is positive, the system of Eq. (27) is *solvable* and its solution $\mathbf{E}/\mathbf{U}$ is *unique*. This would be the situation when solving the damage mechanical problem for a given (frozen) distribution of damage, with $d<1$.

Note that the irreducible form of the problem is easily proved to be numerically stable because of ellipticity of the corresponding bilinear form, while stability has to be enforced for the mixed form. In fact, this enforcement consists of adding a subscale which is constructed using the irreducible solution.

For the nonlinear problem, these stability and solvability properties reflect on the corresponding linearized iterations, as discussed for the irreducible formulation. Therefore, once $\mathbf{E}^{(0)}/\mathbf{U}^{(0)}$ and the iterative procedure are specified, and if convergence is achieved, a solution $\mathbf{E}/\mathbf{U}$ is obtained. Nevertheless, different iterative procedures or different initial estimates may yield different solutions.

3.2.2. Nonlinearity, convergence and uniqueness

The stabilized mixed form of the strain localization problem is *materially nonlinear*, because of the dependence of the constitutive tensor $\mathbf{C}$ (for instance, in the case of the isotropic damage model, through the dependence of $\mathbf{C}$ upon damage variable d, see Chapter 2).

The implications of this nonlinearity are the same discussed for the irreducible form, namely, lack of uniqueness, convergence difficulties, loss of global structural stability and possible lack of correlation between the behavior of the continuous and discrete systems.

4. Strain localization in 1D

In this section the implications that nonlinearity has on the solution of the displacement discontinuity or strain localization problem will be illustrated in a 1D example. Discretization error poses no additional difficulties in this case and, therefore, discussion may focus in the *exact solutions* of the corresponding continuous and discrete problems. Lack of uniqueness and loss of global structural stability are emphasized.

For the following discussion it is not necessary to make it explicit if the material softening behavior is defined in terms of a stress vs displacement jump or a stress vs strain law. The first would correspond to a strong discontinuity approach and the second one to a weak discontinuity or smeared approach. Even if both formulations present several theoretical and technical differences, in 1D it is relatively easy to switch from one to the other [27].

Consider the axial stretching of a bar of length L as the one shown in Fig. 1. The test is conducted under displacement control, that is, an increasing right-end displacement is imposed and the left-end reaction force is evaluated. The cross section of the bar is A and the material behavior is defined by the elastic modulus E, the tensile strength σ_o and the tensile fracture energy $\mathcal{G}_f$. Linear strain-softening is assumed.

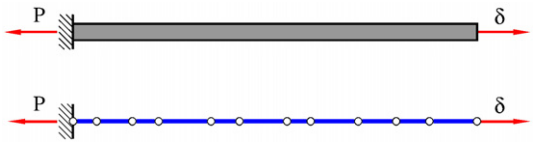

Fig. 1. Stretching of a 1D bar. Continuous and discrete models.

Let us first consider the behavior of a *perfect continuous* model of the bar. Before reaching the peak load, point B in Fig. 2, the problem is linear and the solution is unique. The slope of the elastic branch is defined by the elastic modulus E and the peak load that the bar can sustain is defined by the values of the cross section A and the tensile strength σ_o. Point B is both a limit point and a bifurcation point. All the sections along the bar reach the strain corresponding to the peak stress at the same time, and after that *each one* may "break" and undergo inelastic deformation or, alternatively, unload elastically. Therefore, there are *infinite post-peak solution branches*, depending on how many sections along the bar take the softening branch at the same time. All these solutions satisfy exactly the equilibrium, compatibility and constitutive equations at each point of the domain and its boundary.

The solutions corresponding to 1, 2, 3 and 4 softening sections are plotted in Fig. 2A. The energy dissipated in each solution is different and directly proportional to the number of softening sections in each solution, because the amount of energy necessary to completely release the stress at each section is defined by the values of the cross section A and the fracture energy $\mathcal{G}_f$. The situation may be more complex, because it is also possible to switch *spontaneously* from one descending branch to another.

The test cannot be conducted under load-control because the post-peak regime is unstable. This is clear in Fig. 2A for branches 2, 3 and 4, with negative slopes. If the elastic energy corresponding to point B is greater than the fracture energy necessary to break one section, that is, if the length of the bar is greater than the material length (see Eq. (12)), $L > \bar{l}_s = (2E\mathcal{G}_f / \sigma_o^2)$, then point B is also a turning point, and the equilibrium path snaps back. Branch 1 in the figure illustrates this situation, while post-peak softening slopes (instantaneous tangent

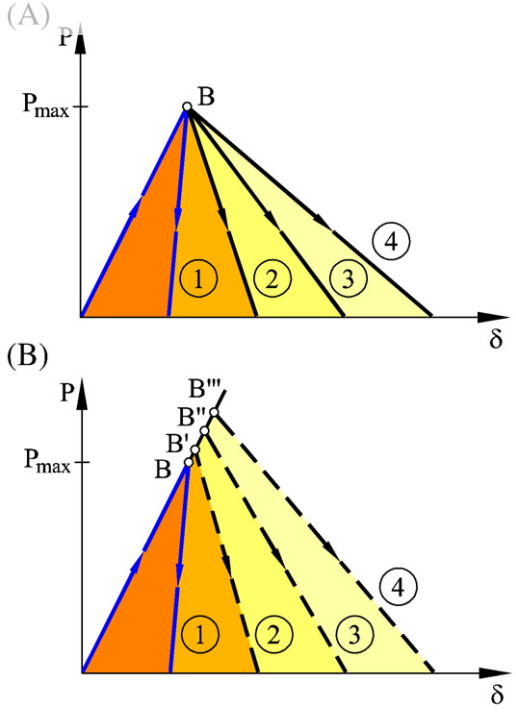

Fig. 2. Stretching of a 1D bar. Response of the (A) perfect and (B) imperfect systems.

Table 1
Order of convergence of different terms in the irreducible and mixed stabilized formulations when interpolations of degree k are used.

Term	Irreducible	Mixed
$\|\|\nabla^s(\mathbf{u}-\mathbf{u}_h)\|\|$	h^k	h^k
$\|\|\mathbf{u}-\mathbf{u}_h\|\|$	h^{k+1} with duality	$h^{k+1/2}$ without duality h^{k+1} with duality
$\|\|\sigma-\sigma_h\|\|$	h^k $(\sigma_h=\mathbf{C}:\nabla^s\mathbf{u}_h)$	$h^{k+1/2}$ without duality h^{k+1} with duality
$\|\|\nabla\cdot(\sigma-\sigma_h)\|\|$	h^{k-1} $(\sigma_h=\mathbf{C}:\nabla^s\mathbf{u}_h)$	h^k

reproduced under displacement control and it requires some form of mixed control.

It is noteworthy that bars of different lengths perform differently, showing degrees of brittleness which are proportional to their physical dimensions. This phenomenon is known as *structural size effect*, and its quantification is, in fact, one of the major practical applications of softening constitutive models and strain localization.

The situation is simpler if we consider an *imperfect continuous* model of the bar. This can be constructed by inserting a section of the bar with a slightly smaller cross section or lower tensile strength or a slightly higher elastic modulus. Now, there is only one *exact* solution to the problem, as this particular section will be the first to meet the inequalities defining inelastic behavior. Point B is now precisely defined by the conditions at this section, and it may still be a limit point and a turning point, but the possibility of bifurcations is eliminated by the structural imperfection. The situation is depicted in Fig. 2B. Note that the other descending branches start at different points such as B', B'' or B''' that are close to point B, at distances that are proportional to the magnitude of the imperfection. If the imperfection is "small", an error in the virtual test could inadvertently produce an inexact solution.

Let us now consider the behavior of a *perfect discrete* model of the bar, constructed by assembly of a finite number of elements of different lengths. For simplicity, let us assume that each element has only one sampling point for the evaluation of the constitutive behavior and constant mechanical properties. Apparently, this system behaves very similarly to the *perfect continuous* model, apart from the fact that now the number of possible post-peak branches is finite. However, this is only true if two premises are met: (A) in the pre-peak regime, the discrete model must be able to represent *exactly* the stress field and (B) in the post-peak regime, the discrete model must be able to represent *exactly* the displacement (and/or strain) and stress fields. If any of these two conditions are not met, the equilibrium curves $P-\delta$ of the continuous and discrete models will be different and the difference may be quantitative and qualitative. Meeting requirements (A) and (B) is not difficult in the simple 1D test proposed, because (A) the stress field is constant all over the domain at all times and (B) there are many ways of modelling a "breaking" section in 1D as exactly as desired.

An *imperfect discrete* model of the bar would also yield a unique solution, but it would only coincide with the corresponding imperfect continuous model if the stated premises are met. Additionally, a perfect discrete system may behave as "imperfect" because of round-off error. This has to be taken into account when working with irreversible nonlinear models defined in terms of inequalities.

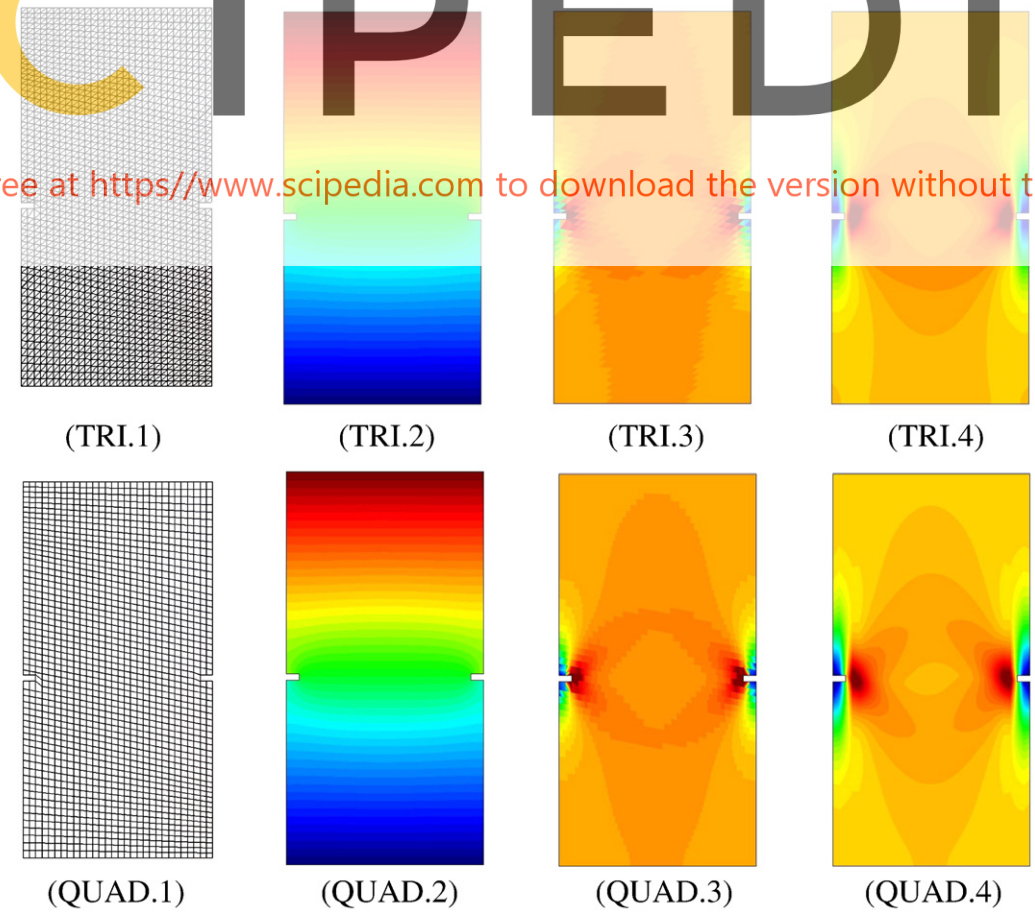

Fig. 3. Results for rectangular strip under tension (top: triangular mesh, bottom: quadrilateral mesh). Contours of: (2) total displacement, (3) major principal strain — irreducible form. (4) major principal strain — stab. mixed form.

5. Strain localization in 2D

The previous section demonstrates that even an apparently simple example of displacement discontinuity or strain localization in 1D may exhibit a relatively complex behavior because of the type of nonlinearity involved. The implications of nonlinearity match in the continuous and discrete models only if the discrete model satisfies two requirements. One is related to the accuracy of the stress field in the discrete model in the pre-localization regime; the other is related to the accuracy of the displacement, strain and the stress fields in the discrete model in the post-localization regime.

Discrete models only yield exact solutions in very particular situations, when the continuous solutions belong to the discrete spaces. Apart from these cases, discrete solutions obtained in different meshes *approximate* the continuous solution. This means that the discrete solutions converge, in a properly defined sense (or norm), to the continuous solution on mesh refinement. Table 1 summarizes the order of convergence that can be expected from the irreducible and the stabilized mixed formulations for different magnitudes of interest in the mechanical problem. This order of convergence depends on the degree of the interpolation functions used in the discrete model. Results from Table 1 imply that the mixed formulation achieves better accuracy on the stresses (or strains) than the irreducible formulation. This may not be considered a discriminating argument, as this improvement is attained at the cost of using more degrees of freedom for the same number of nodes in the FE mesh.

But rate of convergence is not the main issue in the case of strain localization problems. The real problem is *lack of convergence*. The norms evaluated in Table 1 are global. Without additional regularity conditions, local estimates of convergence are expected to be one order smaller. This means that, using linear elements, convergence for the stresses (or strains) cannot be guaranteed in the irreducible formulation. Propitiously, the stabilized mixed formulation can guarantee first order convergence. Using higher order elements in problems involving strong gradients and/or discontinuities does not improve the convergence estimates, since higher order derivatives involved in these estimates are not bounded in such situations. In fact, if the continuous solution is singular, not even the first order derivatives are going to be point-wise bounded. Nevertheless, convergence (without order) can be expected in the mixed formulation in the energy norm defined for a region around the singularity. This is not the case for the irreducible formulation.

Given the *intrinsic local nature* of the strain localization problem, the discrete solution is largely affected by the *local discretization error*. In 2D and, obviously, 3D situations local discretization error affects both the pre and post strain localization regimes. This fact, inherent to the discretization process, is probably the major specific challenge in their solution, and it adds to the difficulties associated to the strongly nonlinear nature of the problem. The usual result of these combined difficulties is that, from all the possible localized solutions that the nonlinear discrete model has, the one obtained is mesh-biased and, therefore, apparently unrelated to the continuous case.

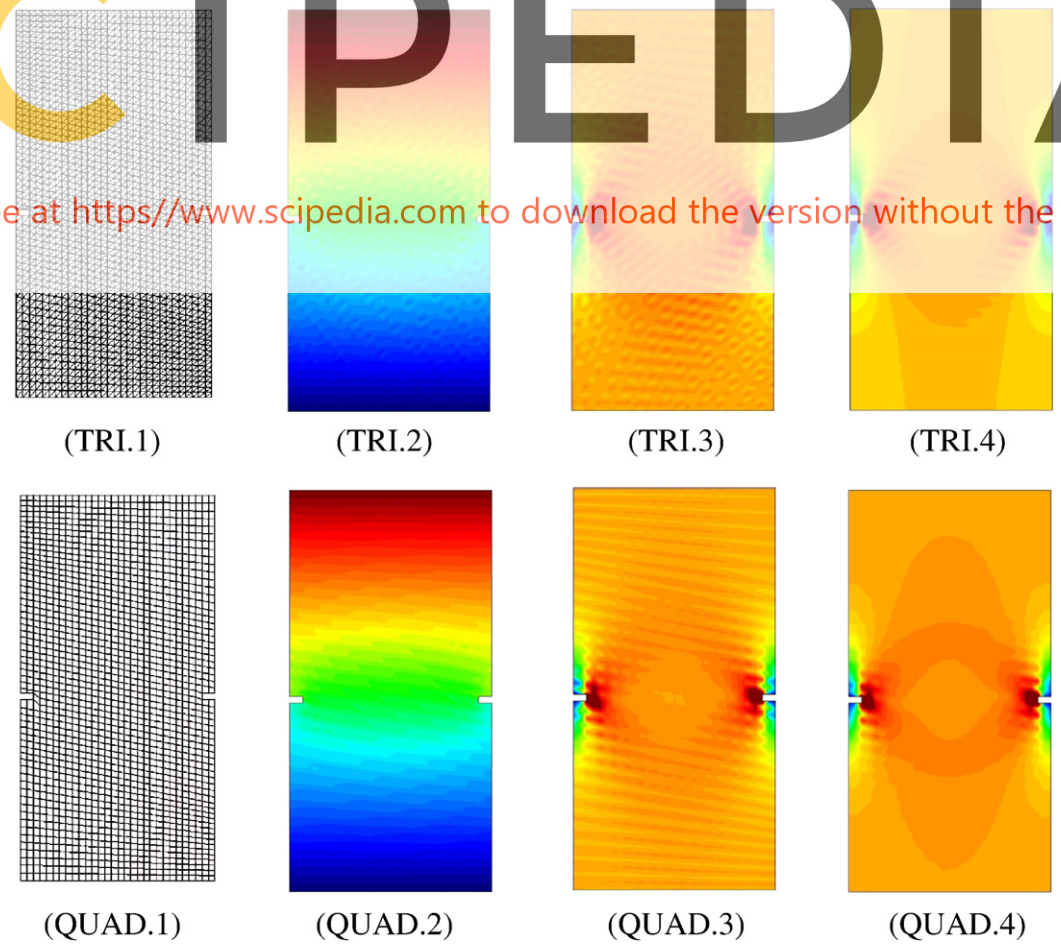

Fig. 4. Results for rectangular strip under tension with the mixed formulation (top: triangular mesh, bottom: quadrilateral mesh). Contours of: (2) total displacement — no stabilization, (3) major principal strain — no stabilization. (4) major principal strain — strain stabilization only.

In the following, the local discretization error both in the pre and post localization regimes is exemplified in 2D situations. The irreducible and mixed formulations are compared to demonstrate the relative benefits of the second approach.

5.1. Local discretization error in the pre-localization regime

Consider the axial stretching of a rectangular doubly notched specimen as the one shown in Fig. 3. A uniform vertical displacement is imposed at the top boundary while the bottom boundary remains fixed. Actual details on the geometry and material properties are given in Section 6, where the same specimen is used for the strain localization analyses.

The solution of the associated continuous elastic problem depends strongly on the actual detail geometry of the tip of the notches. The strain and stress fields are regular if the tips are rounded, but they become singular if the notches present sharp corners. In this case, the corresponding discrete model will perform satisfactorily in terms of a global error norm, but will approximate very poorly the actual behavior at the singular points (see, for instance, Example 5.3 in Part I [22]). In fact, local error estimates will be unbounded. This may be of crucial importance in a nonlinear analysis if the criteria for initiation of inelastic behavior are established in terms of local values and directions or strains or stresses, as it is common in Continuum Mechanics.

Let us illustrate these considerations on the proposed 2D test. Four FE discrete models of the problem are constructed using *P1* triangles (linear displacement), *P1P1* triangles (linear displacement and strain), *Q1* quadrilaterals (bilinear displacement), *Q1Q1* quadrilaterals (bilinear displacement and strain), and the corresponding elastic analyses are performed.

Fig. 3 shows results obtained with the four FE models. The second column, Fig. 3 TRI.2 and QUAD.2, shows contours of the displacement field obtained with the *P1* and *Q1* elements, respectively. Both are very similar to the displacement solutions obtained with the corresponding *P1P1* and *Q1Q1* elements (not shown). In the third column, Fig. 3 TRI.3 and QUAD.3 show contours of the major principal strain field obtained with the *P1* and *Q1* elements, respectively. Note that they are inter-element discontinuous and much significant differences can be appreciated between them in the areas close to the tip of the notches. These are precisely the points where nonlinear behavior leading to strain localization is bound to initiate. In the fourth column, Fig. 3 TRI.2 and QUAD.2 show contours of the major principal strain field obtained with the *P1P1* and *Q1Q1* elements, respectively. Note that they are inter-element continuous and much smoother behavior can be appreciated in the areas close to the tip of the notches. The differences that can still be appreciated between them indicate that the discretization error associated to this level of mesh refinement is small but noticeable.

For the sake of completeness Fig. 4 shows plots that help to understand the need for stabilizing the proposed mixed formulation. In the second column, Fig. 4 TRI.2 and QUAD.2 show contours of the displacement fields obtained with the *P1P1* and *Q1Q1* mixed elements, respectively, *without any stabilization*. The fact that the inf-sup condition is not satisfied effectively causes that the standard Galerkin procedure

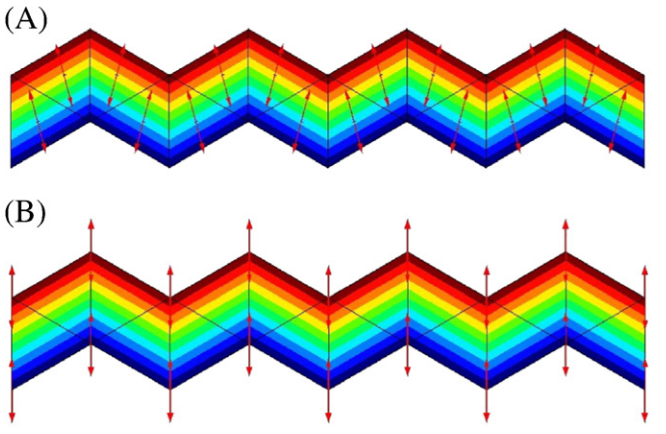

Fig. 5. Separation mode in a band of equal size triangles: (A) Gaussian strains (irreducible formulation), (B) nodal strains (mixed formulation).

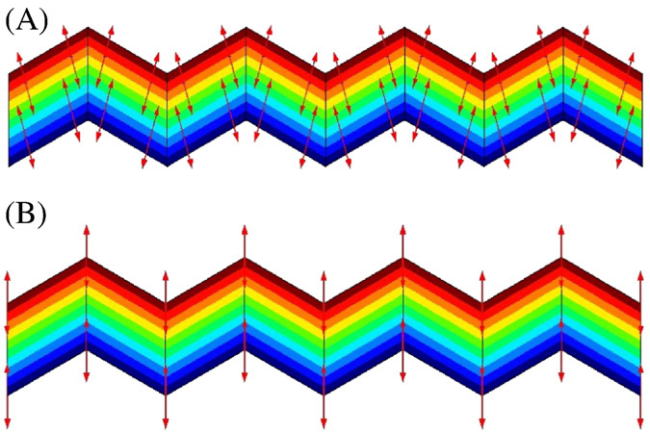

Fig. 6. Separation mode in a band of equal size quadrilaterals: (A) Gaussian strains (irreducible formulation), (B) nodal strains (mixed formulation).

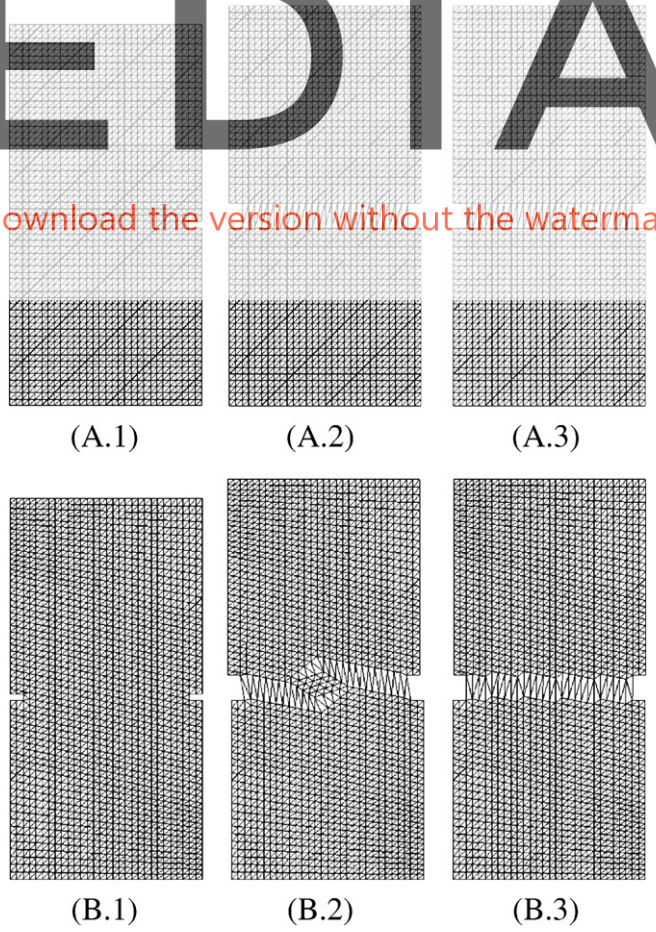

Fig. 7. Triangular meshes A and B for the rectangular strip under tension: (1) undeformed shape, (2) deformed shape — irreducible form, (3) deformed shape — stabilized mixed form.

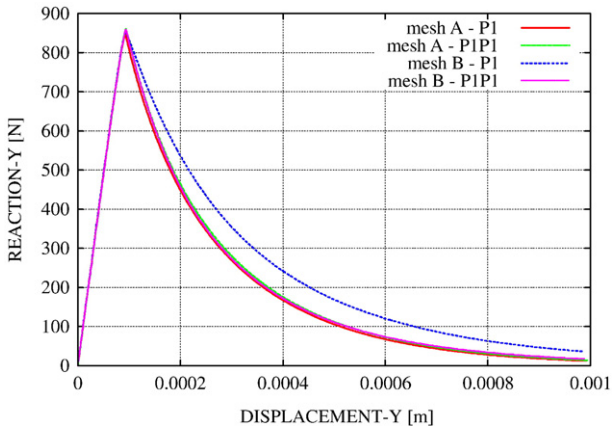

Fig. 8. Vertical reaction versus vertical displacement in rectangular strip under tension using triangular elements P1 and P1P1.

be unstable and this instability shows as oscillations in the displacement field. The third column, Fig. 4 TRI.3 and QUAD.3, shows the corresponding contours of the major principal strain field obtained with the unstable *P1P1* and *Q1Q1* mixed elements, respectively. The results are obviously oscillatory. The fourth column, Fig. 4 TRI.4 and QUAD.4, shows contours of the major principal strain field obtained with the *P1P1* and *Q1Q1* elements, respectively, *stabilized only with the term corresponding to the strain subscale*. In this case the displacement solution (not shown) is stable. Note that the strain field is globally stable, but oscillations can still be appreciated in the neighborhood of the notches. When the terms corresponding to the displacement subscale are added, the strain field is virtually free of oscillations, as shown in Fig. 3 TRI.4 and QUAD.4.

The local discretization error in the elastic or pre-localization regime observed in the presented example cannot be circumvented by regularizing the geometry of the specimen so that singular points are eliminated from the geometry. Even if the tips of the notches in the specimen are rounded and the discrete elastic solution is reasonably accurate, the problem of a local discretization error will reappear as soon as sudden, brittle and irreversible inelastic behavior occurs and strain localization bands progress through the finite element mesh.

The degree of these difficulties is alleviated if regularization techniques are used. Because the difficulties are due to the discretization error, the regularization techniques must be associated to the discretization procedure. *A successful regularization technique should reduce the numerical difficulties of the discrete problem without essentially changing the nature of the solution and be convergent on mesh refinement.* These requirements rule out some techniques such as, for instance, viscous material models or non-local formulations, because they change the nature of the problem and are not related to the discretization procedure.

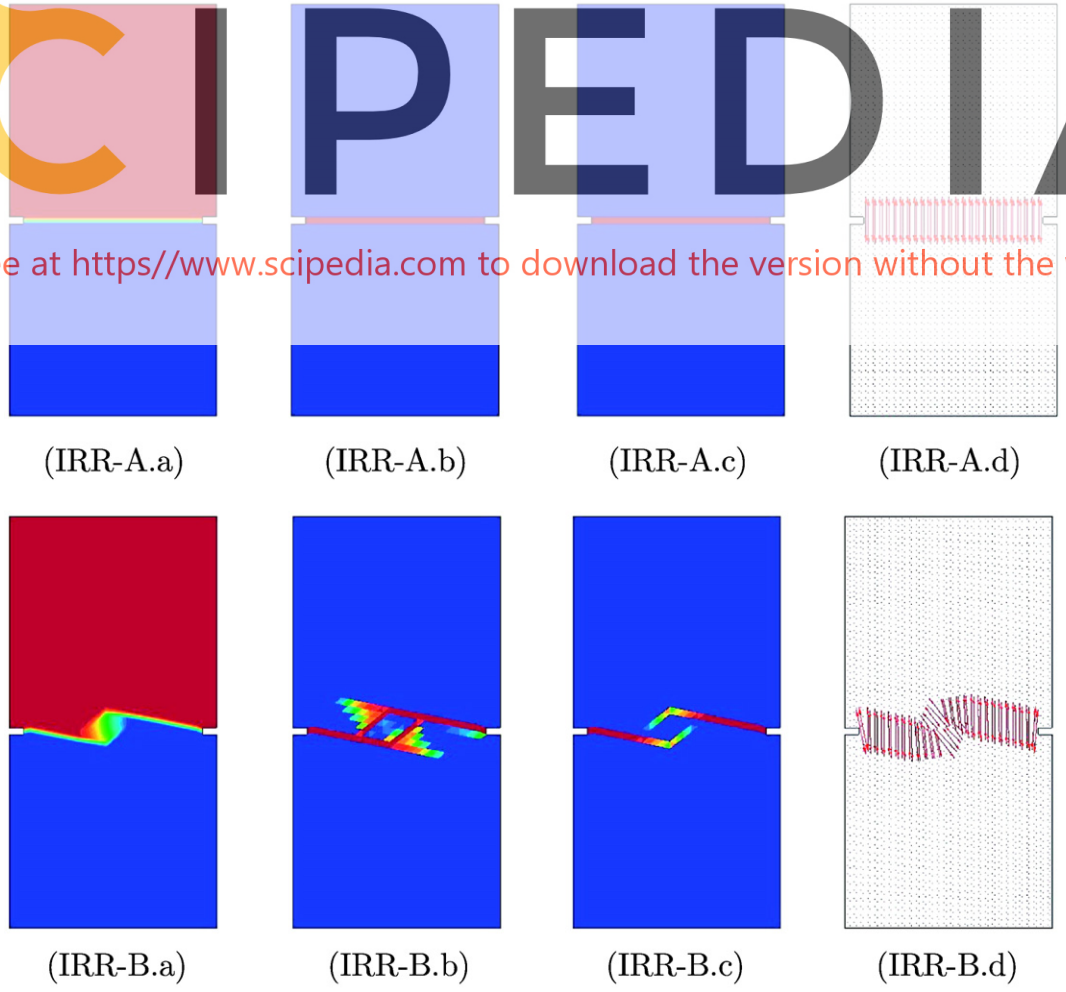

Fig. 9. Results for rectangular strip under tension using the irreducible formulation and triangular meshes (top: mesh A, bottom: mesh B). Contours of: (a) total displacement, (b) damage index (c) major principal strain. (d) Vectors of major principal strain.

These strategies have to be understood as modifications of the original constitutive law.

An additional remark to be made is that strain localization processes can be very different with regard to the propagation mechanisms involved, and this fact has its reflection on the associated numerical difficulties. For instance, tensile cracks usually propagate starting from points with strong tensile stress gradients; in any case, the tip of a progressing crack is always a point of strong stress gradients. So, tensile crack problems are particularly difficult from the discretization error point of view. On the contrary, shear discontinuities or slip lines usually form by progressive narrowing of shear bands. Consequently, prediction of failure mechanisms associated to slip lines is relatively less prone to suffer from *local* discretization error.

In relation to this, let us remark on the use of *auxiliary tracking techniques* in strain localization problems. In the last decade, these procedures, originated in the context of FE applications of the Fracture Mechanics Theory, have been introduced in Continuum Mechanics based approaches to cracking and strain localization problems, even if there is no variational justification for their use. Successful application of the strong discontinuity approach (SDA) and of the X-FEM requires their use to determine the direction of crack propagation ([28–32]). Mosler and Meschke [30] have reported that, without tracking, the SDA leads to the same spurious mesh bias dependence as the standard weak discontinuity approach. Cervera and Chiumenti ([33,34]) have reported in the reciprocal sense that if tracking is used, the weak discontinuity formulation produces results that do not suffer from mesh bias dependence in an evident spurious way.

There are at least two reasons to explain why the use of auxiliary tracking procedures is useful. On one hand, global tracking techniques help to overcome the local discretization error, particularly if coarse meshes are used. On the other hand, more fundamentally, the use of seeding and tracking techniques, either local or global, is determinant in eliminating undesired alternative solutions of the nonlinear discrete problem. The tracking procedures not only "label" the elements along the potential localization path; they also "cross out" the elements outside that path, overriding the possibility of, supposedly spurious, alternative solutions. In this sense, they are useful in selecting the appropriate solution among the many possible ones. This only demonstrates that the "right" solution is there to be tracked down. Regretfully, and disregarding their heuristic introduction, crack tracking techniques are simply not robust enough in cases like bending, where the trajectories of tensile principal strains stop at the neutral axis; and they are intrinsically unable to deal with branching situations which may have physical meaning.

5.2. Local discretization error in the post-localization regime

The second reflection of the local discretization error in the solution of displacement discontinuity and strain localization problems is the incapacity of standard finite elements to reproduce separation modes adequately. It is clear that discrete solution spaces

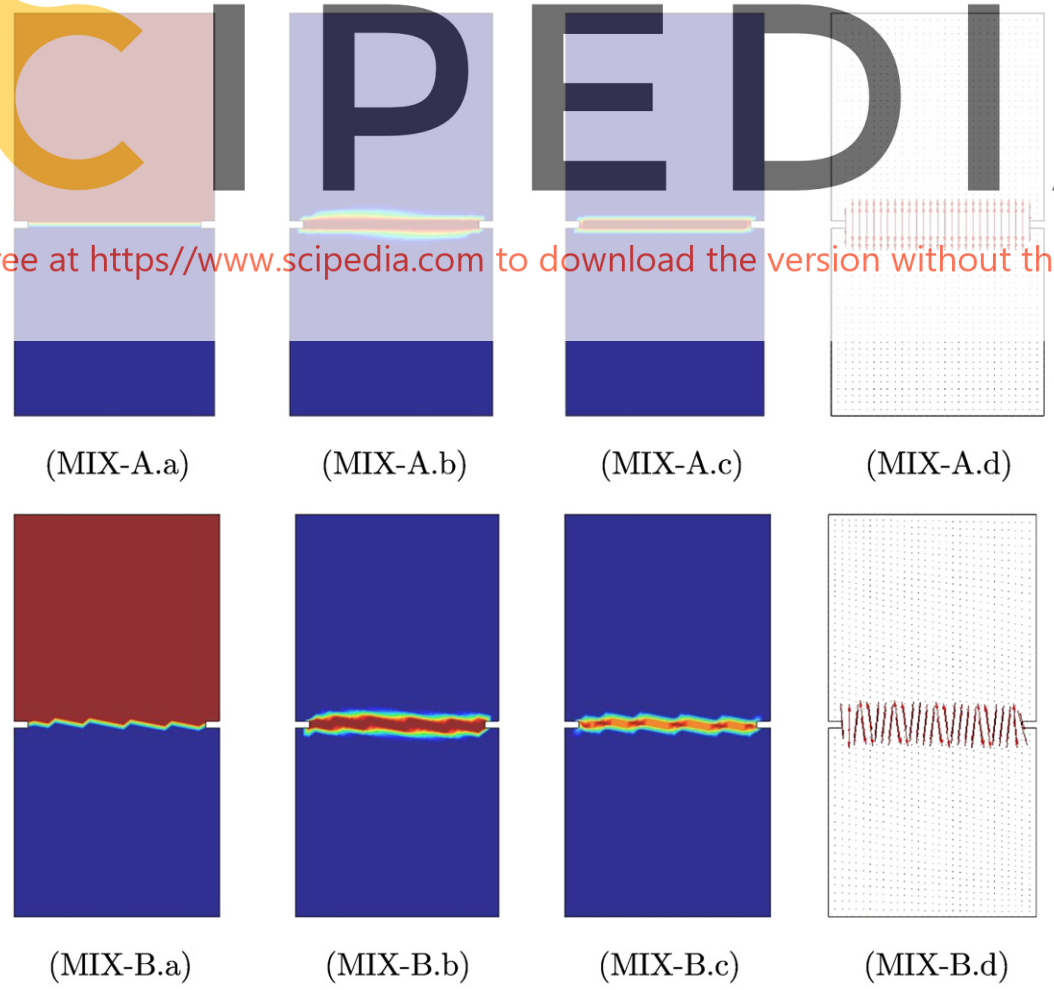

Fig. 10. Results for rectangular strip under tension using the mixed formulation and triangular meshes (top: mesh A, bottom: mesh B). Contours of: (a) total displacement, (b) damage index (c) major principal strain. (d) Vectors of major principal strain.

built from continuous polynomials cannot represent displacement (or strain) discontinuities inside the element. This is purely an *approximability* shortage of the discrete solution spaces used, and it is not related to stability problems of the formulation.

These considerations concerning the very limited ability of standard finite elements to reproduce separation modes in general circumstances are the reason behind the spurious shear locking exhibited by classical smeared orthotropic cracking models [35], which led to their practical neglection by the academic community in the late 1990s. They were substituted by scalar damage and plasticity models which still suffered from spurious shear straining, but largely avoided that this reflected on the stress field.

Let us illustrate this with another 2D test, designed to evaluate the ability of low order elements to represent a displacement discontinuity and, therefore, a separation mode. The problem consists in projecting a unit vertical displacement jump that occurs along a horizontal line. The analytical solution consists in only vertical strains and stresses.

Firstly, a FE discrete model of the problem is constructed using 3-node triangles with *P1* lineal displacement interpolation in the irreducible formulation and *P1P1* linear strain/displacement interpolation in the mixed formulation (see Fig. 5). The model represents a zig-zag band of elements crossed by a horizontal displacement discontinuity. The inclination of the sides of the band is $\pm 30°$. Vertical displacements are set to 0 for the nodes at the bottom of the band and to 1 at the top nodes, horizontal displacements are set to 0 for all nodes. Poisson's ratio is set to 0 for simplicity. Note that none of the elements presents any side orthogonal to the imposed vertical displacement field.

Fig. 5 shows the results obtained in the band in terms of displacement contours and directions of the main tensile strains. Fig. 5A shows the Gaussian principal tensile stresses obtained with the standard irreducible displacement formulation. Note how the computed strains, instead of being vertical, present a inclination that exactly bisects the angle between the correct vertical solution and the normal to the sides of the band ($\pm 15°$). Fig. 5B shows the nodal tensile strains obtained with the mixed strain/displacement formulation proposed in Part I of this work. Here, the strain field is exactly as expected at all nodes.

Secondly, a similar FE discrete model of the problem is constructed using 4-node quadrilaterals with *Q1* linear displacement interpolation in the irreducible formulation and *Q1Q1* linear strain/displacement interpolation in the mixed formulation (see Fig. 6). The geometry of the band of elements and the imposition of the boundary conditions are identical to the previous case. Fig. 5 shows corresponding results obtained in the band in terms of contours of displacements and directions of the main tensile strains. Observe the similarity of these results with the ones obtained if the band is discretized using 3-node triangles.

Even if the added strain continuity of the mixed formulation is partially effective to alleviate the poor behavior exhibited by the low order continuous elements, it is not specifically introduced to make up for these deficiencies. In the case shown, exact results are obtained with the aid of the multiple symmetries of the test.

The effective way of correcting this *approximability* local discretization error is to enrich the approximation spaces with additional degrees of freedom (dofs) that enhance the desired capacities for representing embedded displacement and/or strain discontinuities. This has to be made with caution because some of the possible strategies may cause new numerical instabilities in the enriched discrete problem.

Recent FE technologies like the SDA ([27,30,36–43]) and the X-FEM ([44–46]) tackle this problem directly. The first one enriches the solution space by introducing discontinuous functions inside the elements, while the second makes use of the partition-of-unity property of the nodal shape functions. The advantage of the SDA is that the additional dofs can be condensed at element level, at the cost of not enforcing inter-element displacement continuity and having to develop special procedures for each type of element. In the X-FEM approach displacements are inter-element continuous and this precludes the possibility of solving the additional dofs separately from the original ones.

Even if these two approaches are very attractive from the theoretical point of view, they are not free from practical inconveniences. In fact, both formulations are often applied in a regularized manner ([47–51]). In these regularized versions, the discrete solution considers embedded strain localization bands rather than actual displacement discontinuities. The width of the regularized band is a numerical parameter, chosen to be "small". An obvious choice for this width is the size of the element, which, on mesh refinement, can be made as small as desired. Apparently, this takes us back to the original concept of the smeared approaches and, in fact, it is exactly so in the 1D case, but this is not true in other contexts.

Combination of the stabilized mixed form presented in this work with a suitable enrichment technique for the displacement and/or strain fields is expected to bring a satisfactory answer to the strain localization problem.

6. Numerical examples

The application of the stabilized strain/displacement $\varepsilon/\mathbf{u}$ formulation presented in Part I of this work to the problem of strain localization is illustrated below by solving two different benchmark problems. Relative performance of the irreducible displacement formulation and the stabilized mixed strain/displacement formulation is tested considering

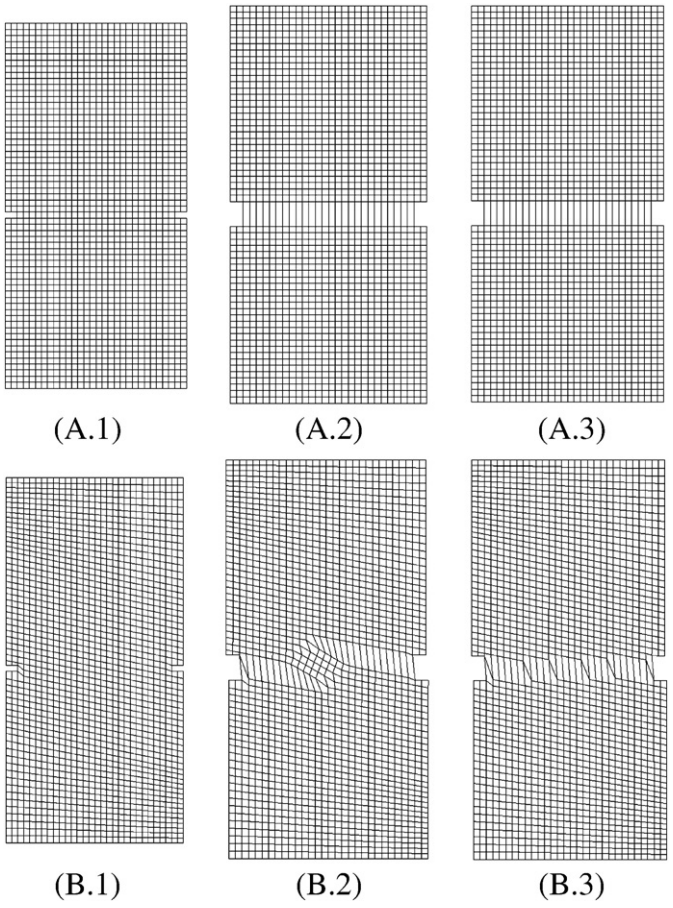

Fig. 11. Quadrilateral meshes A and B for the rectangular strip under tension: (1) undeformed shape, (2) deformed shape — irreducible form, (3) deformed shape — stabilized mixed form.

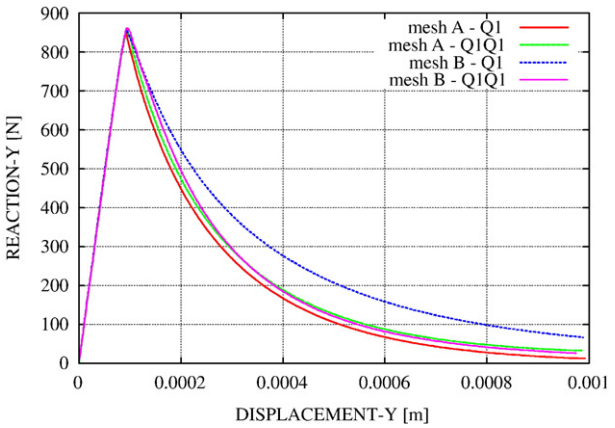

Fig. 12. Vertical reaction versus vertical displacement in rectangular strip under tension using quadrilateral elements Q1 and Q1Q1.

2D 3-node triangular and *4-node quadrilateral* meshes. The elements used will be: *P1* (linear displacement), *P1P1* (linear strain/ linear displacement), *Q1* (bilinear displacement), *Q1Q1* (bilinear strain/bilinear displacement). Only low order elements are considered because they are more effective in problems involving sharp displacement and strain gradients. However, the proposed approach is very general. When the stabilized mixed strain/displacement formulation is used, values $c_\varepsilon = 1.0$ and $c_u = 1.0$ are taken for the evaluation of the stabilization parameters τ_ε and τ_u, respectively. We have chosen $C_{\min} = (1-d)E$, understanding that the Young's modulus E is a characteristic value of the elastic tensor (constants appearing in the minimum eigenvalue of the elastic tensor may be included in the algorithmic constant c_u in Eq. (10) of Part I).

In all examples, strain localization is induced by the local scalar damage model with exponential strain softening described in Section 2. The following material properties are assumed: Young's modulus $E = 2$ GPa, Poisson's ratio $\nu = 0.0$, tensile strength $\sigma_o = 1$ MPa and mode I fracture energy $\mathcal{G}_f = 250$ J/m^2.

The discrete problem is solved incrementally, in a (pseudo)time step-by-step manner. Analyses are performed under displacement control in order to trace the complete post-peak behavior. An automatic time incrementation procedure is used to reduce the size of the time steps when convergence due to the nonlinear effects is more difficult. Within each step, a modified Newton–Raphson method, together with a line search procedure, is used to solve the corresponding non-linear system of equations. Convergence of a time step is attained when the ratio between the norm of the iterative and the incremental norm of the residual arrays is lower than 10^{-3}. It has to be remarked that no tracking algorithm of any sort has been used in any of the computations.

Calculations are performed with an enhanced version of the finite element program COMET [52], developed at the International Center for

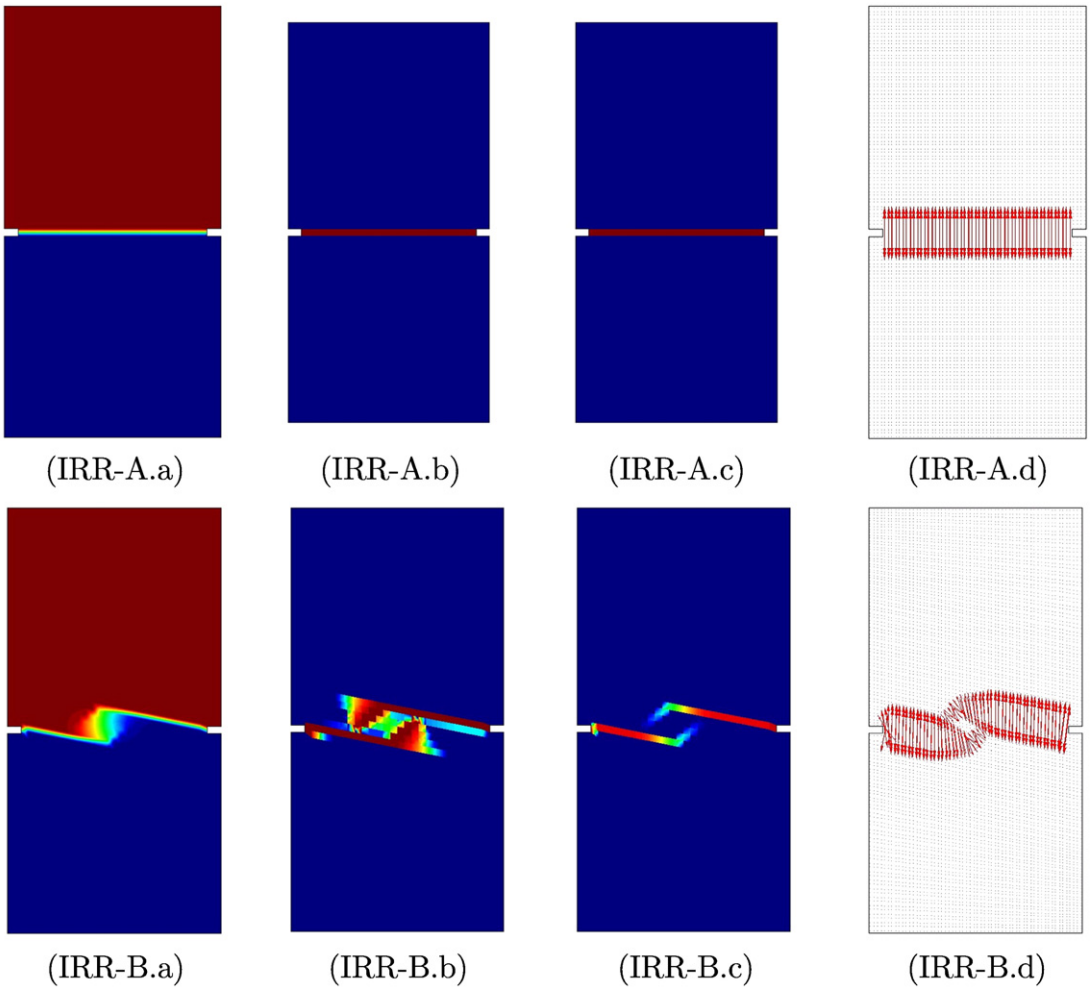

Fig. 13. Results for rectangular strip under tension using the irreducible formulation and quadrilateral meshes (top: mesh A, bottom: mesh B). Contours of: (a) total displacement, (b) damage index (c) major principal strain. (d) Vectors of major principal strain.

Numerical Methods in Engineering (CIMNE). Pre and post-processing is done with GiD, also developed at CIMNE [53].

6.1. Rectangular strip under tension

The first example is a plane rectangular strip subjected to axial vertical stretching applied by imposing null vertical displacements at the bottom and increasing a uniform vertical displacement at the top. Dimensions of the strip are 100×200 mm$\times$mm (width$\times$height) and the thickness of the strip is 10 mm. For the evaluation of the stabilization parameters in the mixed formulation, the width of the strip, $L_0=$ 100 mm, is taken as representative length of the problem.

For a perfectly rectangular strip, the elastic solution involves linear vertical displacements and constant vertical strains and stresses in the whole domain, and no unique strain localization solution exists as the stretching is increased. Two symmetrical notches are introduced close to the horizontal axis of symmetry of the strip to perturb the constant strain and stress fields and to ensure uniqueness of the strain localization problem.

This example is selected because it represents a sort of patch test for pure mode I fracture. On one hand, the stress field is almost constant before damage and it should remain so after localization. On the other hand, the almost constant initial strain field bifurcates into two different strain fields inside and outside the localization band after damage. At the end of the localization process, the apparent displacement jump across the band must be *constant*.

The example is used to assess the ability of the *irreducible* (IRR) and *mixed* (MIX) formulations to reproduce these ideal conditions and the dependence of the obtained results with respect to the mesh-bias.

6.1.1. Triangular meshes: P1 and P1P1 elements

Let us start by considering triangular finite element meshes. The rectangular notched domain is discretized in two different structured meshes of triangles with different preferential alignments. On one hand, mesh A (Fig. 7A.1) consists of rectangular triangles with predominant directions at 0°, +45° and +90° with the horizontal axis. As the strip is expected to damage along a horizontal line, the elements in this mesh have one of their sides parallel to the damage band. On the other hand, mesh B (Fig. 7B.1) also consists of almost rectangular triangles, but the mesh is "slanted" on purpose, so that the predominant directions are −13°, +32° and +90° with the horizontal axis. Therefore, the elements in this mesh do not have any of their sides parallel to the expected strain localization band. Both meshes consist of about 1,800 nodes and 3,600 elements, with a relation $L_0/h=40$.

The computed deformed shapes of the strip using meshes A and B with the *irreducible formulation* are shown in Fig. 7A.2 and B.2, respectively (imposed vertical displacement $\delta=1.0$ mm, with a displacement amplification factor of 10). As shown, the localization band obtained with mesh A follows exactly a horizontal line, and the deformation mode obtained is globally correct. Results are very different for mesh B. Here one damage band starts from each notch at

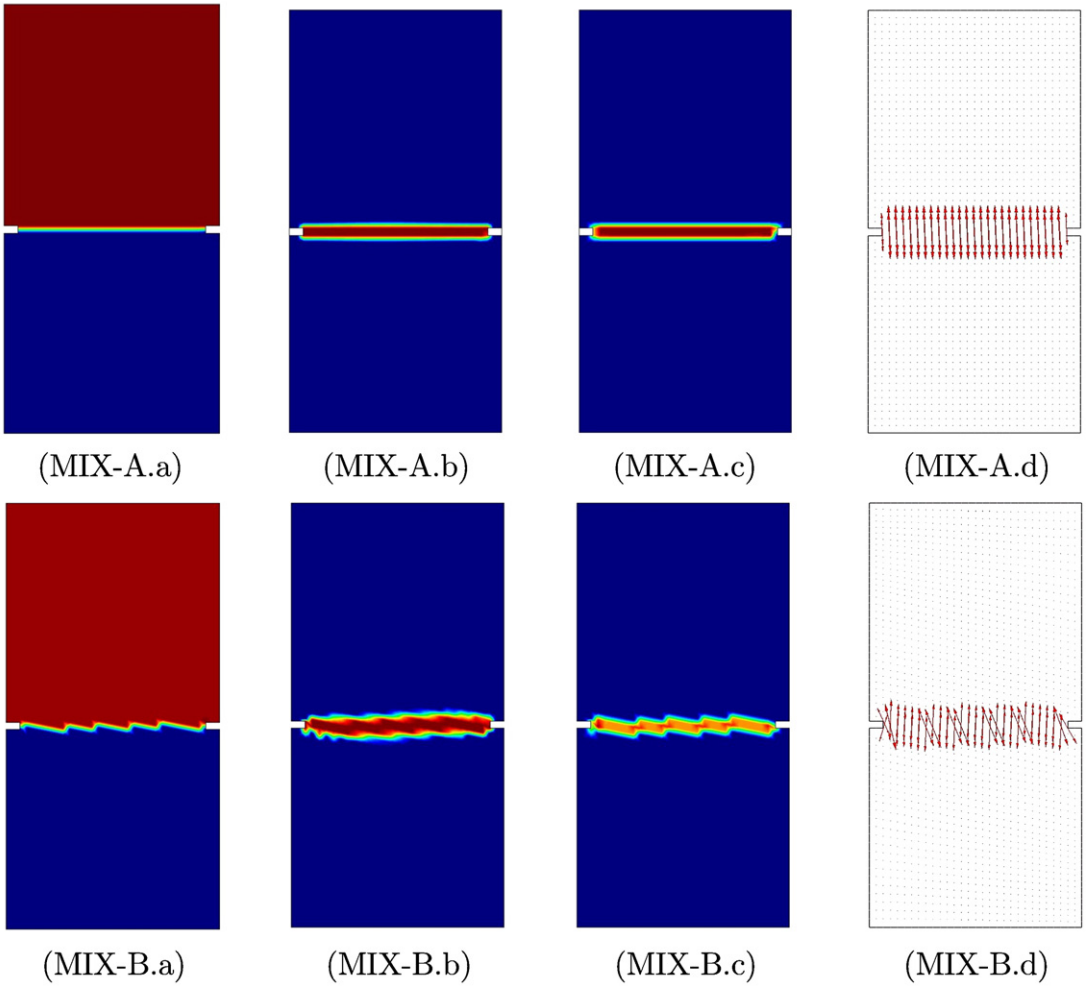

Fig. 14. Results for rectangular strip under tension using the mixed formulation and quadrilateral meshes (top: mesh A, bottom: mesh B). Contours of: (a) total displacement, (b) damage index (c) major principal strain. (d) Vectors of major principal strain.

an angle which is spuriously determined by the mesh bias. These two extension bands do not meet at the centre and they only change direction at a very advanced stage of the localization process.

Correspondingly, Fig. 7A.3 and B.3 depict the deformed shapes obtained using meshes A and B with the *stabilized mixed formulation*. The localization band computed in mesh A, which is "properly" aligned, follows exactly a horizontal line, and the global deformation mode obtained is correct. Remarkably, the global deformation mode obtained for mesh B, despite its strong unfavorable mesh-bias, is also correct. Here, the localization band zig-zags through the mesh to reproduce the expected horizontal "crack".

Fig. 8 shows the load vs displacement curves obtained with both the *irreducible* and the *stabilized mixed* formulations using the two meshes. Note how three of the four results virtually overlap, and only the curve corresponding to the *irreducible* formulation on mesh B shows a different behavior. The trend corresponds with the deformed shapes of Fig. 7. Results obtained with the *stabilized mixed* formulation in both meshes A and B are correct, both in terms of peak-load and dissipated energy, showing no spurious mesh-bias dependence.

Let us consider in some detail the behavior of the two formulations. Fig. 9 shows different results obtained with the *irreducible* formulation on both meshes, when the localization band is well developed, for imposed vertical displacement $\delta = 1.0$ mm. The first column shows contours of total displacement, the second column shows contours of the damage index, the third column shows contours of the major principal strain, and the last column shows vectors of this major principal strain.

The differences between the top row, corresponding to results obtained on mesh A, with the bottom row, corresponding to results obtained on mesh B, are evident. The solution showed on the top row is correct in every aspect. However, results on the bottom row differ significantly. The first column shows displacement jumps across two main localization bands, whose directions spuriously follow the mesh alignment. The reason for this has to be sought in the pre-localization discretization error referred to in the previous Section. The second and third columns show corresponding contours of the damage index and of the major principal strain, where the same strongly mesh dependent behavior is evident. The last column shows vectors of the major principal strain. Here, it can be clearly observed how the irreducible solution is severely affected by the post-localization discretization error.

Fig. 10 shows the corresponding results obtained with the *stabilized mixed* formulation on both meshes, for the same imposed vertical displacement $\delta = 1.0$ mm. In this case, the differences between the top row, corresponding to mesh A, with the bottom row, corresponding to mesh B, are quite smaller. The solution showed on the top row is in very good correspondence with the one obtained with the same mesh and the irreducible formulation. The only differences between them can be seen in the damage and strain contours, where the mixed solution is slightly more "spread" due to the inter-elemental continuity of the strain field. More interesting are the results of the second row, where the mixed solution on mesh B shows displacement jumps across only one zig-zagging localization band, which is horizontal in average, successfully avoiding the unfavorable alignment of the mesh. The second and third columns show contours of the damage index and of the major principal strain, and the same satisfactory behavior is observed. Note how the contours of strain are optimally localized, with the maximum resolution of the mesh. The last column shows vectors of the major principal strain. Here, it can be observed that the localized strains resulting from the mixed formulation are also affected by the post-localization discretization error, but being the localization band correctly located, the averaged effect of this error is diminished.

To interpret the results shown in Fig. 10, it has to be taken into account that they correspond to the final stage of the simulation. Then, displacements are totally localized, and strains, obtained from the discrete geometric equation, likewise. However, damage has been evolving monotonically during the whole process and it shows a slightly more spread profile corresponding to less localized previous stages. Results would show less smearing on mesh refinement.

6.1.2. Quadrilateral meshes: Q1 and Q1Q1 elements

Let us now consider quadrilateral finite elements. To this end, the rectangular domain is discretized in two different structured meshes of quadrilaterals with different preferential alignments. The two meshes are obtained from the meshes of triangles used before, by joining adequately every two adjoining triangles to form a quadrilateral. Therefore, both meshes have the same number of nodes and nodal locations as before, and exactly half number of elements. On one hand, mesh A (Fig. 11A.1), consists of squares with predominant directions at 0° and +90° with the horizontal axis. As the strip is expected to damage along a horizontal line, the elements in this mesh have one of their sides parallel to the damage band. On the other hand, mesh B (Fig. 11B.1) also consists of almost square quads, but the mesh is purposely "slanted", so that the predominant directions are −13° and +77° with the horizontal axis. Therefore, the elements in this mesh do not have any of their sides parallel to the expected strain localization band. Both meshes consist of about 1800 nodes and 1800 elements, with a relation $L_0/h = 40$.

The example is used to assess the ability of the *irreducible* (IRR) and *mixed* (MIX) formulations to reproduce *constant* displacement jumps in quadrilateral discretizations and the dependence of the obtained results with respect the mesh-bias.

The computed deformed shapes of the strip using meshes A and B with the *irreducible formulation* are shown in Fig. 11A.2 and B.2, respectively. As expected, the localization band obtained with mesh A

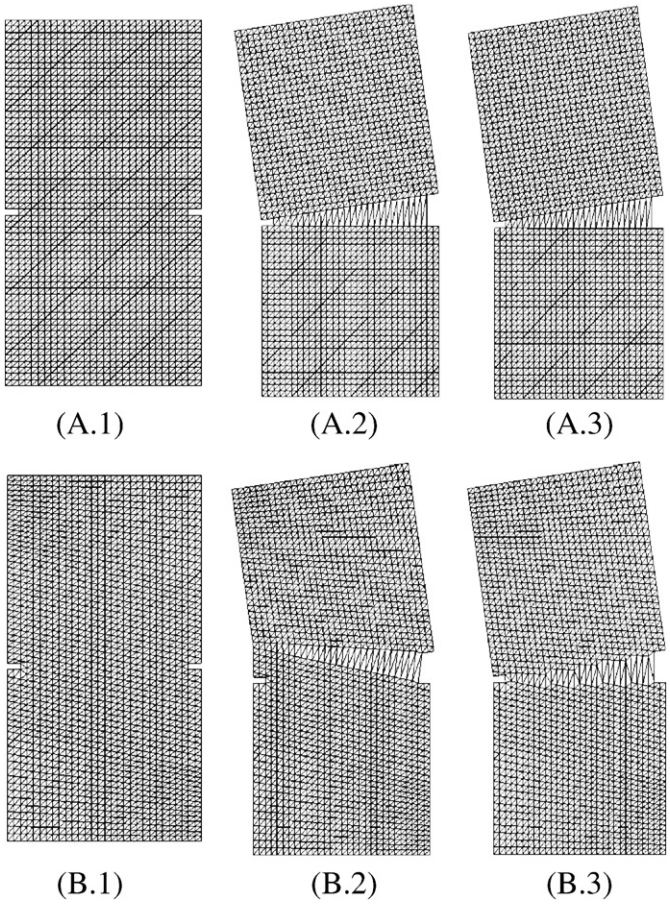

Fig. 15. Triangular meshes A and B for the rectangular strip under tension and bending: (1) undeformed shape, (2) deformed shape — irreducible form, (3) deformed shape — stabilized mixed form.

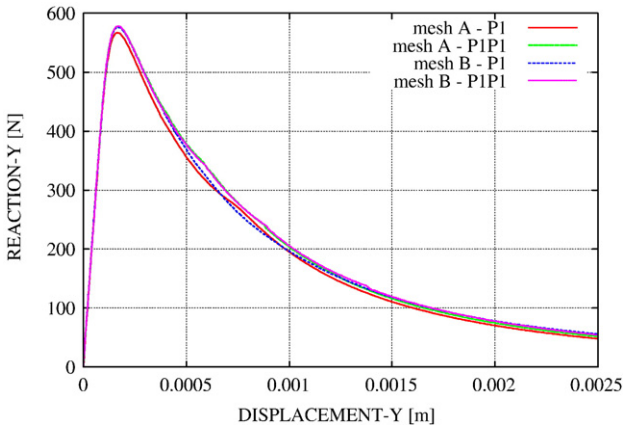

Fig. 16. Vertical reaction versus maximum vertical displacement in rectangular strip under tension and bending using triangular elements P1 and P1P1.

is exactly horizontal, and the deformation mode obtained is correct. Contrariwise, results are very unsatisfactory for mesh B. Here, mesh bias is evident in the deformed geometry, with two damage bands starting from the lateral notches at angles which are spuriously determined by the mesh alignment.

Fig. 11A.3 and B.3 show, respectively, the computed deformed shapes of the strip using meshes A and B with the *mixed formulation*. As in the case with triangular finite elements, results obtained with mesh A are, as expected, correct. Noteworthier are the results obtained with the "unfavorable" mesh B, where the two forming localization bands progresses zig-zagging through the mesh until they correctly meet at the centre of the specimen. It has to be recalled that no tracking algorithm has been used in the computations.

Fig. 12 shows the load vs displacement curves obtained with both the *irreducible* and the *stabilized mixed* formulations using the two quadrilateral meshes A and B. Results are very similar to those shown in Fig. 7, corresponding to the triangular elements. The trend of the different curves corresponds to the deformed shapes of Fig. 11. Results obtained with the *stabilized mixed* formulation in both meshes A and B are correct, both in terms of peak-load and dissipated energy, showing no spurious mesh-bias dependence. They are slightly more dissipative than the corresponding reference result because of the inter-element continuity of the strains and the extended bandwidth of quadrilateral meshes.

Fig. 13 shows different results obtained with the *irreducible* formulation on both meshes, when the localization band is well developed. The differences between the top row, corresponding to results obtained on mesh A, with the bottom row, corresponding to results obtained on mesh B, are evident.

Fig. 14 shows the corresponding results obtained with the *stabilized mixed* formulation on both meshes. Comments on these two figures are very similar to those referred to Figs. 9 and 10, corresponding to the triangular meshes. This also applies to the apparent mismatch between the strongly localized displacement field and the more spread strain and damage fields.

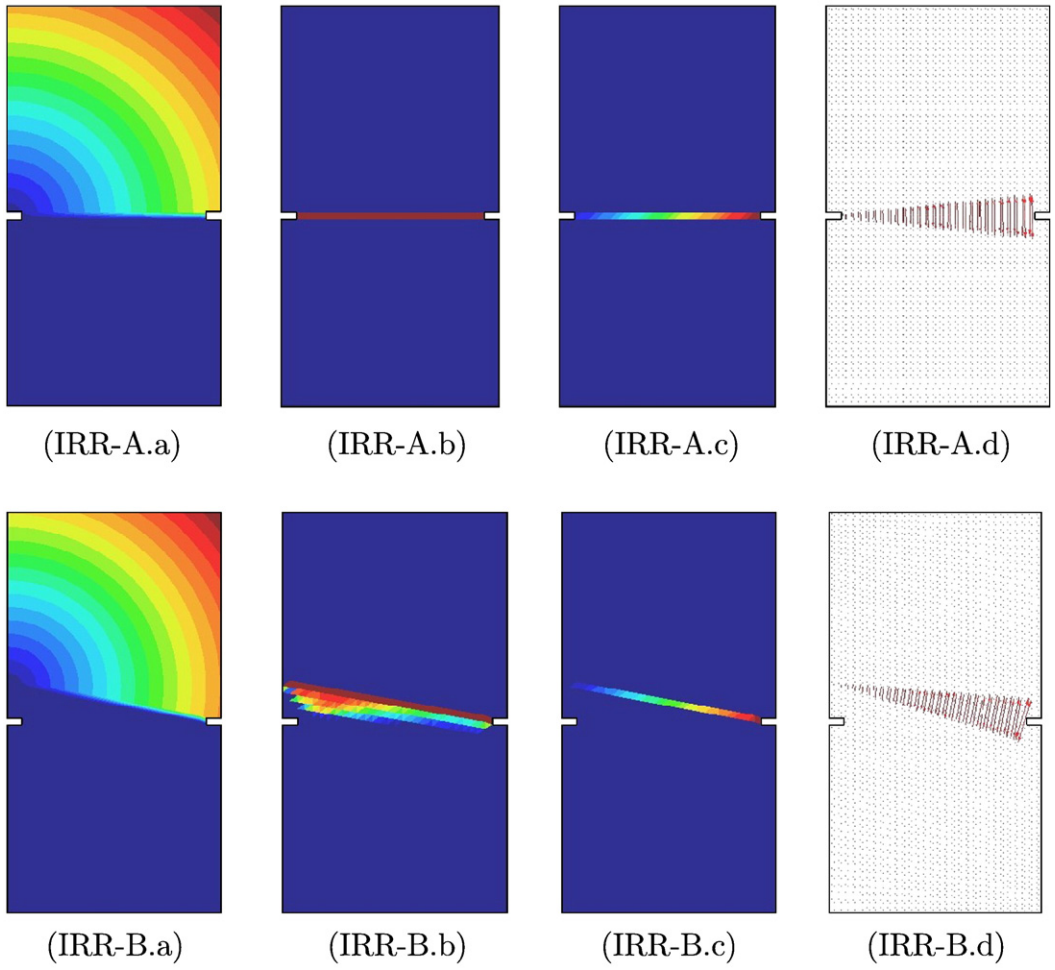

Fig. 17. Results for rectangular strip under tension and bending using the irreducible formulation and triangular meshes (top: mesh A, bottom: mesh B). Contours of: (a) total displacement, (b) damage index (c) major principal strain. (d) Vectors of major principal strain.

6.2. Rectangular strip under tension and bending

The second example is a plane rectangular strip subjected to axial vertical stretching and bending applied by imposing null vertical displacements at the bottom and increasing vertical displacements at the top that vary linearly, from a value of 0 at the left end to a maximum value at the right end. Dimensions of the strip are 100×200 mm $\times$ mm (width $\times$ height) and the thickness of the strip is 10 mm. For the evaluation of the stabilization parameters in the mixed formulation, the width of the strip, $L_0 = 100$ mm, is taken as representative length of the problem.

For a perfectly rectangular strip, the elastic solution is an identical linear distribution of strains and stresses along each horizontal section of the strip and, therefore, there is no unique localization solution as the bending is increased. As in the previous example, two symmetrical notches are introduced close to the horizontal axis of symmetry of the strip to ensure a unique localization band.

Consequently, the expected unique solution is a horizontal band of damaged elements that starts at the right notch and progresses horizontally towards the left notch. Because no compressive vertical stresses must develop, tensile damage must progressively affect the whole notched section of the specimen, and form a horizontal localization band that spans from right to left. Vertical strains must progressively localize inside this band. Apparent displacement jumps across the band must be *linear*.

The example is used to assess the ability of the *irreducible* (IRR) and *mixed* (MIX) formulations to reproduce these ideal conditions and the dependence of the obtained results with respect the mesh-bias. The test is far more demanding that the previously presented case (pure stretching), because the simulation of linear displacement jumps occurring across bands formed by low order triangular and quadrilateral finite elements requires some attention ([41,43]). In the case of linear *P1* triangles, the corresponding strain field is constant over the element. More conveniently, the linear *P1P1* triangle incorporates a linear strain field that can naturally accommodate a linear displacement jump in a smeared fashion. The situation is similar for quadrilateral *Q1* and *Q1Q1* elements, although far more complex to analyze for general configurations of the quadrilaterals.

6.2.1. Triangular meshes: P1 and P1P1 elements

Let us start by considering triangular finite elements. The rectangular domain is discretized in the same two different structured meshes of triangles used for the pure tension test. Recall that mesh A (Fig. 15A.1) consists of rectangular triangles with predominant directions at 0°, +45° and +90° with the horizontal axis, while mesh B (Fig. 15B.1) is "slanted" so that the predominant directions are −13°, +32° and +90° with the horizontal axis.

The computed deformed shapes of the strip using meshes A and B with the *irreducible formulation* are shown in Fig. 15A.2 and B.2, respectively (maximum imposed vertical displacement $\delta = 0.3$ mm, with a displacement amplification factor of 5). As shown, the localization band obtained with mesh A follows exactly a horizontal line, and the deformation mode obtained is correct. Results are obviously incorrect for mesh B, where the damage band progresses at

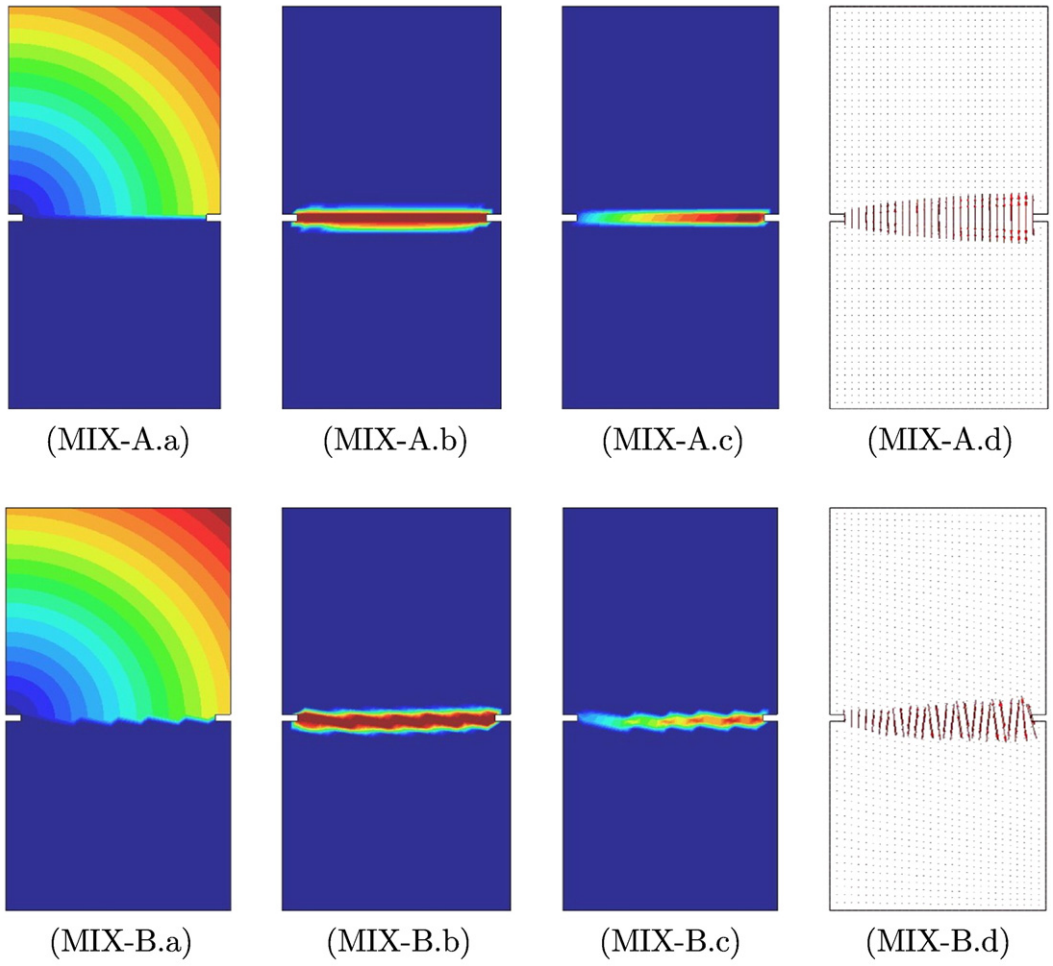

Fig. 18. Results for rectangular strip under tension and bending using the mixed formulation and triangular meshes (top: mesh A, bottom: mesh B). Contours of: (a) total displacement, (b) damage index (c) major principal strain. (d) Vectors of major principal strain.

an angle that is totally determined by the mesh bias. This localization band never reaches the notch at the left end.

Correspondingly, Fig. 15A.3 and B.3 show, respectively, the computed deformed shapes of the strip using meshes A and B with the *mixed formulation*. Again, correct global deformation patterns are obtained for both mesh alignments: the localization band starts at the right-end notch and progresses horizontally through the mesh until it reaches the notch at the left-end.

Fig. 16 shows the load vs displacement curves obtained with both the *irreducible* and the *stabilized mixed* formulations using the two triangular meshes. In this case, all the four curves are very close, and the severe misbehavior of the *irreducible* formulation on mesh B does not show on this plot. Results obtained with the *stabilized mixed* formulation in both meshes A and B are correct, both in terms of peak-load and dissipated energy; they are slightly more dissipative than the corresponding reference result because of the inter-element continuity of the strain field.

Figs. 17 and 18 give some further insight into the behavior of the two formulations. Fig. 17 shows results obtained with the *irreducible* formulation on both meshes. The differences between the top row, corresponding to results obtained on mesh A, with the bottom row, corresponding to results obtained on mesh B, are evident. The solution showed on the top row is correct in every aspect, the displacement and strain contours consistent with a *linear* displacement jump across the correctly solved horizontal localization band. Results on the bottom row differ from these very much. Even if the first column shows a clear displacement jump across a unique localization band and the strain contours in the third column are consistent with this, the prediction of this "crack" is definitely determined by the spatial discretization. Scatter of the damage contours in the second column denotes unsuccessful attempts of the solution process to find alternative branches. In the last column, the incorrect direction of the vectors of the major principal strain demonstrates the incapacity of the triangles to accurately represent the vertical displacement jump across the inclined localization band.

Fig. 18 shows the corresponding results obtained with the *stabilized mixed* formulation on both meshes. The concordance between the top row, corresponding to mesh A, with the bottom row, corresponding to mesh B, is remarkably good. Both solutions are also in good correspondence with the one obtained with mesh A and the irreducible formulation. The main differences between these three correct solutions are due to the inter-elemental continuity of the strain field of the mixed formulation. Note how results obtained for mesh B are optimally localized, given the resolution of the mesh. This can be appreciated in the displacement and strain contour plots. The last column shows vectors of the major principal strain. Like in the irreducible case, the localized strains resulting from the mixed formulation are affected by the post-localization discretization error, but being the localization band correctly located and aligned, the averaged effect of this error is greatly diminished.

6.2.2. Quadrilateral meshes: Q1 and Q1Q1 elements

Let us finally consider quadrilateral finite elements for the bending test. The rectangular domain is discretized in the same two different structured meshes of quadrilaterals used for the pure tension test. Recall that, mesh A (Fig. 19A.1) consists of squares with predominant directions at 0° and +90° with the horizontal axis, while mesh B (Fig. 19B.1) is constructed so that the predominant directions are −13° and +77° with the horizontal axis.

The computed deformed shapes of the strip using meshes A and B with the *irreducible formulation* and the *mixed formulation* are shown in the second and third columns of Fig. 19, respectively. As it can be seen, results are very similar to those obtained with the triangular meshes and shown in Fig. 15, although the deformation pattern obtained in the last case depicted is noteworthy.

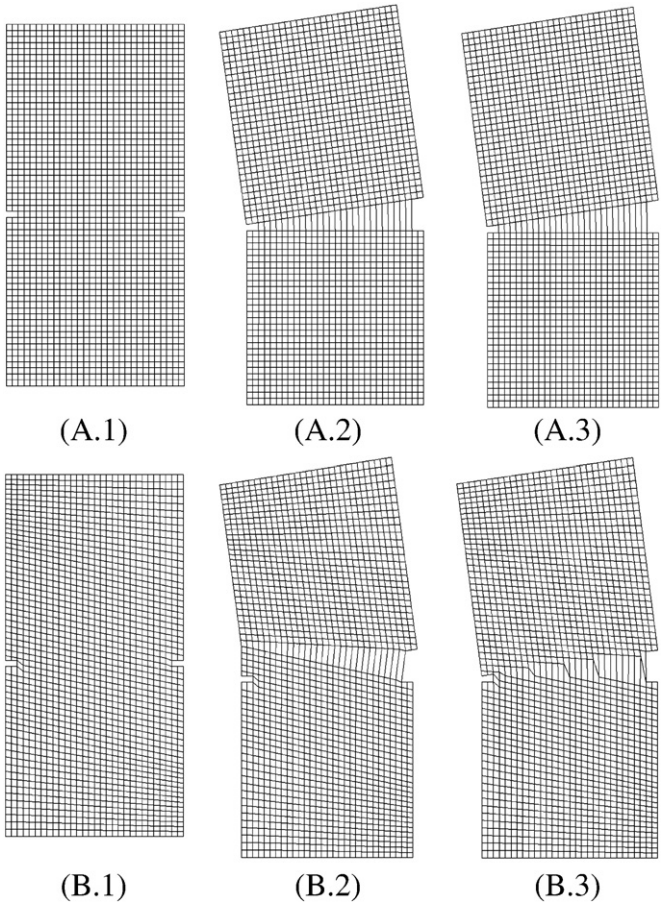

Fig. 19. Quadrilateral meshes A and B for the rectangular strip under tension and bending: (1) undeformed shape, (2) deformed shape — irreducible form, (3) deformed shape — stabilized mixed form.

Fig. 20 shows the load vs displacement curves obtained with both the *irreducible* and the *stabilized mixed* formulations using the two quadrilateral meshes. Again, all the four curves are very close, because the incorrect failure mechanism produced by the *irreducible* formulations on mesh B does not stand out on this plot. Results obtained with the *stabilized mixed* formulation in both meshes A and B are correct, although they predict a slightly higher peak load than the corresponding result obtained with the irreducible formulation. This is due to the inter-element continuity of the strains and the extended

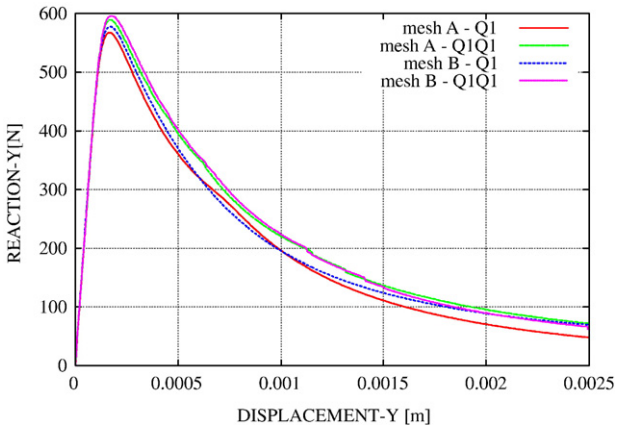

Fig. 20. Vertical reaction versus maximum vertical displacement in rectangular strip under tension and bending using quadrilateral elements Q1 and Q1Q1.

bandwidth of quadrilateral meshes. This collateral effect is reduced on mesh refinement.

As in the pure tension case, results corresponding to displacement, damage and principal strain distributions at failure are very similar to those obtained for the triangular meshes (Figs. 17 and 18) and are omitted.

7. Conclusions

This paper deals with the question of strain localization associated with materials which exhibit softening due to tensile straining. The analysis of both the irreducible and the mixed continuous and discrete forms of the problem shows that both are satisfactorily stable in terms of global norms of displacements and strains. Lack of uniqueness of the solution is solely associated with the strong nonlinear nature of the problem. Therefore, the well-known observed mesh-bias dependence of the results obtained using the standard irreducible formulation is attributed to lack of convergence of local values of the strains and stresses. This complication is solved using the fully stable formulation of the mixed equal order strain/displacement mechanical problem described in Part I of this work. Low order finite elements with continuous strain and displacement fields (triangular *P1P1* and quadrilateral *Q1Q1*) and a standard *local* isotropic Rankine damage model with strain-softening are used for this purpose. The derived method yields a *general* and *robust* scheme, suitable for engineering applications.

The proposed formulation is shown to attain satisfactory control on the displacement and strain fields, removing global and local oscillations induced by the geometry of the mesh. This translates in the achievement of three goals:

- a significant reduction of the local error in the pre-localization regime, ensuring convergence of the strain values at local level,
- the position and orientation of the localization bands are independent of the directional bias of the finite element mesh, without the need to resorting to *ad hoc* crack tracking techniques, and
- a correct global structural load-deflection response in the post-peak regime.

Benchmark numerical examples show the substantial advantage of the mixed formulation over the irreducible one to predict correct failure mechanisms with localized patterns of strain, virtually free from any dependence of the mesh directional bias.

Acknowledgment

Financial support from the Spanish Ministry for Education and Science under the *SEDUREC* project (CSD2006-00060) is acknowledged.

References

[1] M. Cervera, M. Chiumenti, Size effect and localization in J_2 plasticity, International Journal of Solids and Structures 46 (2009) 3301–3312.
[2] Z.P. Bazant, J. Planas, Fracture and Size Effect in Concrete and Other Quasibrittle Materials, CRC Press, Boca Raton, 1998.
[3] R. de Borst, Simulation of strain localization: a reppraisal of the Cosserat continuum, Engineering Computations 8 (1991) 317–322.
[4] P. Steinmann, K. Willam, Localization witin the framework of micropolar elastoplasticy, in: V. Mannl, et al., (Eds.), Advances in Continuum Mechanics, Springer Verlag, Berlin, 1992, pp. 296–313.
[5] E.C. Aifantis, On the microstructural origin of certain inelastic models, Transactions ASME Journal of Engineering Materials Technology 106 (1984) 326–330.
[6] I. Vardoulakis, E.C. Aifantis, A gradient flow theory of plasticity for granular materials, Acta Mechanica 87 (1991) 197–217.
[7] R. de Borst, H.B. Mulhaus, Gradient-dependent plasticity: formulation and algorithm aspect, Int. J. Num. Meths. in Engng. 35 (1992) 521–539.
[8] Pamin, J. (1994). Gradient-Dependent Plasticity in Numerical Simulation of Localization Phenomena. Ph. D. Thesis, TU Delft, The Netherlands.
[9] R.H.J. Peerlings, R. de Borst, W.A.M. Brekelmans, M.G.D. Geers, Gradient-enhanced damage modelling of concrete failures, Mechanics of Cohesive-Frictional Materials 4 (1998) 339–359.
[10] G. Pijaudier-Cabot, Z.P. Bazant, Nonlocal damage theory, Journal of Engineering Mechanics, ASCE 113 (10) (1987) 1512–1533.
[11] G. Pijaudier-Cabot, A. Huerta, Finite element analysis of bifurcation in nonlocal strain softening solids, Comp. Meth. in Applied Mech. and Engrg. 90 (1991) 905–919.
[12] M. Jirásek, Nonlocal models for damage and fracture: comparison of approaches, Int. J. Solids and Structures 35 (1998) 4133–4145.
[13] R. de Borst, Some recent issues in computational failure mechanics, Int. J. Num. Meths. in Eng. 52 (2001) 63–95.
[14] Z. Bazant, M. Jirásek, Nonlocal integral formulations of plasticity and damage: survey of progress, J. Eng. Mechanics, ASCE 128 (2002) 1119–1149.
[15] A. Needelman, Material rate dependence and mesh sensitivity in localization problems, Comp. Meth. in Appl. Mech. and Eng. 67 (1987) 68–75.
[16] M. Chiumenti, Q. Valverde, C. Agelet de Saracibar, M. Cervera, A stabilized formulation for incompressible elasticity using linear displacement and pressure interpolations, Comp. Meth. in Appl. Mech. and Eng. 191 (2002) 5253–5264.
[17] M. Cervera, M. Chiumenti, Q. Valverde, C. Agelet de Saracibar, Mixed linear/linear simplicial elements for incompressible elasticity and plasticity, Comp. Meth. in Appl. Mech. and Eng. 192 (2003) 5249–5263.
[18] M. Cervera, M. Chiumenti, C. Agelet de Saracibar, Softening, localization and stabilization: capture of discontinuous solutions in J2 plasticity, Int. J. for Num. and Anal. Meth. in Geomechanics 28 (2003) 373–393.
[19] M. Cervera, M. Chiumenti, C. Agelet de Saracibar, Shear band localization via local J_2 continuum damage mechanics, Comp. Meth. in Appl. Mech. and Eng. 193 (2003) 849–880.
[20] M. Chiumenti, Q. Valverde, C. Agelet de Saracibar, M. Cervera, A stabilized formulation for incompressible plasticity using linear triangles and tetrahedra, Int. J. of Plasticity 20 (2004) 1487–1504.
[21] C. Agelet de Saracibar, M. Chiumenti, Q. Valverde, M. Cervera, On the orthogonal subgrid scale pressure stabilization of finite deformation J_2 plasticity, Comp. Meth. in Appl. Mech. and Eng. 195 (2006) 1224–1251.
[22] M. Cervera, M. Chiumenti, R. Codina, Mixed stabilized finite element methods in nonlinear solid mechanics, Comput. Methods Appl. Mech. Eng. (2010), doi:10.1016/j.cma.2010.04.006.
[23] Z.P. Bazant, B.H. Oh, Crack band theory for fracture of concrete, Materials and Structures 16 (1983) 155–177.
[24] J. Oliver, A consistent characteristic length for smeared cracking models, Int. J. Num. Meth. Engng. 28 (1989) 461–474.
[25] J.C. Simo, R.L. Taylor, Consistent tangent operators for rate-independent elasticity-plasticity, Comp. Meth. in Appl. Mech. and Eng. 48 (1985) 101–118.
[26] J.C. Simo, R.L. Taylor, A return mapping algorithm for plane stress elastoplasticity, Int. J. Num. Meths. in Engng. 22 (1986) 649–670.
[27] J.C. Simo, J. Oliver, F. Armero, An analysis of strong discontinuities induced by strain-softening in rate-independent inelastic solids, Computational Mechanics 12 (1993) 49–61.
[28] J. Oliver, A.E. Huespe, E. Samaniego, W.V. Chaves, Continuum approach to the numerical simulation of material failure in concrete, Int. J. for Num. and Anal. Meth. in Geomechanics 28 (2004) 609–632.
[29] J. Oliver, A.E. Huespe, Continuum approach to material failure in strong discontinuity settings, Comp. Meth. in Appl. Mech. and Eng. 193 (2004) 3195–3220.
[30] J. Mosler, G. Meschke, Embedded crack vs. smeared crack models: a comparison of elementwise discontinuous crack path approaches with emphasis on mesh bias, Comp. Meth. in Appl. Mech. and Eng. 193 (2004) 3351–3375.
[31] C. Feist, G. Hofstetter, An embedded strong discontinuity model for cracking of plain concrete, Comp. Meth. in Appl. Mech. and Eng. 195 (2006) 7115–7138.
[32] G. Meschke, P. Dumstorff, Energy-based modeling of cohesive and cohesionless cracks via X-FEM, Comp. Meth. in Appl. Mech. and Eng. 196 (2007) 2338–2357.
[33] M. Cervera, M. Chiumenti, Smeared crack approach: back to the original crack, Int. J. for Num. and Anal. Meth. in Geomechanics 30 (2006) 1173–1199.
[34] M. Cervera, M. Chiumenti, Mesh objective tensile cracking via a local continuum damage model and a crack tracking technique, Comp. Meth. in Appl. Mech. and Eng. 196 (1–3) (2006) 304–320.
[35] M. Jirásek, T. Zimmermann, Analysis of rotating crack model, Journal of Engineering Mechanics (ASCE) 124 (8) (1998) 842–851.
[36] J. Oliver, Continuum modeling of strong discontinuities in solid mechanics using damage models, Computational Mechanics 17 (1995) 277–296.
[37] J. Oliver, M. Cervera, O. Manzoli, Strong discontinuities and continuum plasticity models: the strong discontinuity approach, Int. J. of Plasticity 15 (1999) 319–351.
[38] M. Jirásek, Comparative study on finite elements with embedded discontinuities, Comp. Meth. in Appl. Mech. and Eng. 188 (2000) 307–330.
[39] J. Mosler, G. Meschke, 3D modelling of strong discontinuities in elastoplastic solids: fixed and rotating localization formulations, Int. J. Num. Meths. in Engng. 57 (2003) 1553–1576.
[40] J. Mosler, A general technique to embed non-uniform discontinuities into standard solid finite elements, Computers and Structures 84 (2005) 742–757.
[41] O.L. Manzoli, P.B. Shing, On the efficient implementation of an elastoplastic damage model for large-scale analyses of material failure: a multiscale approach, Computers and Structures 83 (2006) 369–382.
[42] J.M. Sancho, J. Planas, D.A. Cendón, E. Reyes, J.C. Gálvez, An embedded cohesive crack model for finite element analysis of concrete fracture, Engineering Fracture Mechanics 74 (1–2) (2007) 75–86.
[43] C. Linder, F. Armero, Finite elements with embedded strong discontinuities for the modeling of failure in solids, Int. J. Num. Meths. in Engng. 72 (2007) 1391–1433.
[44] T. Belytschko, T. Black, Elastic crack growth in finite elements with minimal remeshing, Comp. Meth. in Appl. Mech. and Eng. 45 (5) (1999) 601–620.
[45] N. Möes, J. Dolbow, T. Belytschko, A finite element method for crack growth without remeshing, Int. J. Num. Meths. in Engng. 46 (1999) 131–150.

[46] N. Sukumar, N. Möes, B. Moran, T. Belytschko, Extended finite element method for three-dimensional crack modelling, Int. J. Num. Meths. in Engng. 48 (2000) 1549–1570.
[47] B. Patzák, M. Jirásek, Process zone resolution by extended finite elements, Engineering Fracture Mechanics 70 (2003) 957–977.
[48] E. Benvenuti, A. Tralli, G. Ventura, A regularized XFEM model for the transition from continuous to discontinuous displacements, Int. J. Num. Meths. in Engng. 74 (2008) 911–944.
[49] E. Benvenuti, A regularized XFEM framework for embedded cohesive interfaces, Comp. Meth. in Appl. Mech. and Eng. 197 (2009) 4367–4378.
[50] M. Cervera, An orthotropic mesh corrected crack model, Comp. Meth. in Appl. Mech. and Eng. 197 (2008) 1603–1619.
[51] M. Cervera, A smeared-embedded mesh-corrected damage model for tensile cracking, Int. J. Num. Meths. in Engng. 76 (2008) 1930–1954.
[52] M. Cervera, C. AgeletdeSaracibar, M. Chiumenti, COMET: COupled MEchanical and Thermal analysis, 2002 Data Input Manual, Version 5.0, Technical report IT-308. Available from <http://www.cimne.upc.es>.
[53] GiD: The Personal Pre and Post Processor, 2009 <http://www.gidhome.com>.